Strain Tuning of Ferroelectric Thin Films*

Darrell G. Schlom,[1,†] Long-Qing Chen,[2]
Chang-Beom Eom,[3] Karin M. Rabe,[4]
Stephen K. Streiffer,[5] and Jean-Marc Triscone[6]

[1]Department of Materials Science and Engineering, Pennsylvania State University, University Park, Pennsylvania 16802-5005; email: schlom@ems.psu.edu

[2]Department of Materials Science and Engineering, Pennsylvania State University, University Park, Pennsylvania 16802-5005; email: lgc3@psu.edu

[3]Department of Materials Science and Engineering, University of Wisconsin, Madison, Wisconsin 53706; email: eom@engr.wisc.edu

[4]Department of Physics and Astronomy, Rutgers University, Piscataway, New Jersey 08854-8019; email: rabe@physics.rutgers.edu

[5]Center for Nanoscale Materials, Argonne National Laboratory, Argonne, Illinois 60439; email: streiffer@anl.gov

[6]DPMC, University of Geneva, 1211 Geneva 4, Switzerland; email: jean-marc.triscone@physics.unige.ch

Annu. Rev. Mater. Res. 2007. 37:589–626

The *Annual Review of Materials Research* is online at http://matsci.annualreviews.org

This article's doi:
10.1146/annurev.matsci.37.061206.113016

1531-7331/07/0804-0589$20.00

*The U.S. Government has the right to retain a nonexclusive, royalty-free license in and to any copyright covering this paper.

[†]To whom correspondence should be addressed.

Key Words

substrates, theory and simulation, ferroelectric characterization methods, epitaxial oxide films, superlattices, multicomponent oxides

Abstract

Predictions and measurements of the effect of biaxial strain on the properties of epitaxial ferroelectric thin films and superlattices are reviewed. Results for single-layer ferroelectric films of biaxially strained $SrTiO_3$, $BaTiO_3$, and $PbTiO_3$ as well as $PbTiO_3/SrTiO_3$ and $BaTiO_3/SrTiO_3$ superlattices are described. Theoretical approaches, including first principles, thermodynamic analysis, and phase-field models, are applied to these biaxially strained materials, the assumptions and limitations of each technique are explained, and the predictions are compared. Measurements of the effect of biaxial strain on the paraelectric-to-ferroelectric transition temperature (T_C) are shown, demonstrating the ability of percent-level strains to shift T_C by hundreds of degrees in agreement with the predictions that predated such experiments. Along the way, important experimental techniques for characterizing the properties of strained ferroelectric thin films and superlattices, as well as appropriate substrates on which to grow them, are mentioned.

INTRODUCTION

All materials are electrostrictive (see p. 600 for sidebar: More on Electrostriction), but in ferroelectrics the quadratic coupling between polarization and strain can be especially strong. This strong polarization-strain coupling is responsible for the changes in the paraelectric-to-ferroelectric transition temperature (T_C, also called the Curie point), piezoelectric coefficients, and dielectric and electrooptic properties when the mechanical boundary conditions of a ferroelectric are altered. It has long been understood that for bulk ferroelectric ceramics and single crystals under Gibbsian conditions of constant pressure, the ferroelectric phase transition temperature is reduced, and the piezoelectric and dielectric properties are strongly modified by the application of hydrostatic pressure (1–3). But for thin films the opportunity arises to apply huge, nonhydrostatic strains well beyond where their bulk counterparts would crack. For sufficiently thin films, biaxial strains[1] of several percent can be tolerated (4, 5; 6, pp. 283–90).[2] Such strains have previously been used to improve the mobility of semiconductors in transistors (7, 8) and to alter the transition temperature of ferromagnetic (9, 10) and superconducting (11–13) materials. Strain-induced enhancements in T_C as large as tens of degrees have been observed for the latter phenomena (9). Although conventional wisdom is that the best possible properties of any ferroelectric are found in a single crystal of that material, the synthesis of highly perfect ferroelectric thin films on suitable substrates has demonstrated that appropriately strained ferroelectric thin films can exhibit properties that are greatly superior to their bulk counterparts. Owing to the strong coupling between strain and ferroelectricity, T_C shifts of hundreds of degrees are expected (14–23) and have been observed (20, 21, 24–30) in strained ferroelectric thin films. The tuning of ferroelectric properties through the application of strain to ferroelectric thin films is the subject of this review. We note that, in addition to the mechanical boundary conditions (strain) discussed here, electrical boundary conditions can also significantly modify the phase transitions, phase stability, and domain structures (31–36).

Strains can be imparted into thin films through differences in lattice parameters and thermal expansion behavior between the film and the underlying substrate, or they can arise from defects formed during film deposition (6, pp. 60–83, 387–461; 37–39). Fully coherent, epitaxial films have the advantage that high densities of threading dislocations [e.g., the $\sim 10^{11}$ dislocations cm^{-2} observed in partially relaxed ferroelectric films (40, 41)] are avoided. The strain field around dislocations locally alters the properties of the film, making its ferroelectric properties inhomogeneous and often degraded (42–44). Because we desire to describe the intrinsic effect of strain on ferroelectric properties, we limit our review to experiments involving fully coherent epitaxial films. This approach is shown schematically in **Figure 1**. To achieve coherent strained films, high-quality substrates are required.

Ferroelectric: a material possessing a macroscopic spontaneous polarization that can be reoriented through the application of an external electric field

Polarization: an electric dipole moment per unit volume (polarization is a vector quantity)

Paraelectric-to-ferroelectric transition temperature (T_C): also known as the Curie point, the temperature of the phase transformation at which a material goes from having no reorientable macroscopic spontaneous polarization (paraelectric) to possessing a spontaneous polarization that can be reoriented through the application of an external electric field (ferroelectric)

Piezoelectric: a linear relationship between an applied electric field and the resulting strain ($\varepsilon \propto E$) in some (so-called piezoelectric) materials

Substrate: the macroscopic base material upon which a film is grown. For epitaxial films this is a wafer of a single crystal that is chemically and structurally compatible with the film to be grown on it

Strain: a symmetric second-rank tensor describing the deformation of a material

---

[1] The biaxial strain $\varepsilon_s = \frac{(a_\parallel - a_0)}{a_0}$, where a_0 is the lattice parameter of the ferroelectric material in its cubic state under stress-free conditions (free-standing) and $a_\parallel$ is the in-plane lattice parameter of the biaxially strained ferroelectric film.

[2] The limit of strain is given by the Griffith criteria for crack formation (4, 5): $\varepsilon_s = (1 - \nu)\sqrt{2\gamma/(\pi\, E\, t)}$, where the film has Poission's ratio ν, surface energy γ, Young's modulus E, and thickness t and the biaxial strain ε_s arises from lattice mismatch with the underlying substrate, i.e., $a_\parallel = a_{\text{sub}}$ for fully coherent epitaxial growth.

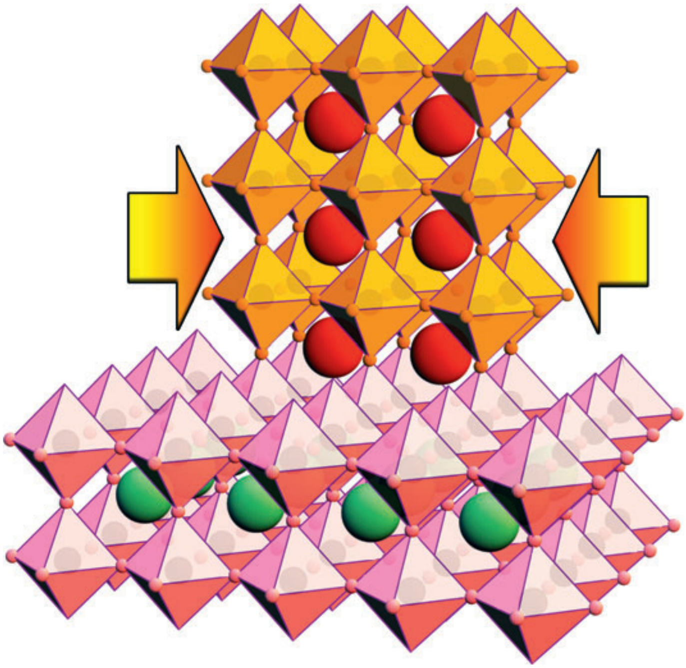

Figure 1

Schematic of a fully coherent epitaxial ferroelectric film biaxially strained to match an underlying substrate. In this example, both the ferroelectric film and substrate have ABO_3 perovskite structures, with the larger A ion (*red* and *green*) nominally centered within a corner-shared framework of octahedra, the smaller B ion nominally centered within these octahedra, and oxygen at the vertices of the octahedra.

After a brief description of the status of available substrates that can be used to strain common ferroelectric materials in thin film form via lattice mismatch, theoretical predictions of the effect of strain on ferroelectric properties are described. These predictions are then compared with experimental observations for (*a*) single-layer ferroelectric films as well as (*b*) superlattices containing ferroelectric layers. Along the way, several important experimental techniques for characterizing the ferroelectric properties of strained ferroelectric thin films and superlattices are described.

SUBSTRATES FOR STRAINING FERROELECTRIC FILMS

The importance of the quality of the underlying crystalline template, on which an epitaxial film is grown, cannot be overemphasized. For conventional semiconductors (e.g., silicon and GaAs), highly perfect single crystals, chemical mechanical polishing, chemical etching methods to prepare smooth and damage-free surfaces for epitaxial growth, and detailed knowledge of surface reconstructions all exist and are a key to the success of semiconductor technology. For the growth of ferroelectric thin films and superlattices, for which it is desired to establish the intrinsic effect of strain on film properties, the availability of appropriate substrates and methods to prepare smooth and highly perfect surfaces on which epitaxial growth is initiated is also crucial.

Superlattice: a sequence of thin film layers whose thickness and order is precisely repeated many times

For oxide ferroelectrics with perovskite structures [e.g., $BaTiO_3$, $(Ba,Sr)TiO_3$, $PbTiO_3$, $Pb(Zr,Ti)O_3$], chemically and structurally compatible perovskite substrate materials are needed. Intensive work on high-temperature superconductors

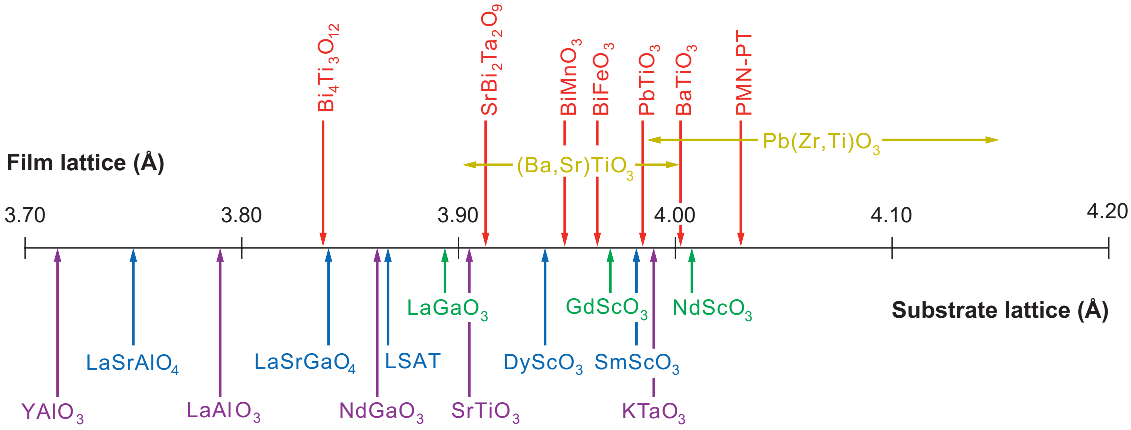

Figure 2

A number line showing the pseudotetragonal or pseudocubic *a*-axis lattice constants (in angstroms) of some ferroelectric perovskites of current interest (*above* the number line) and of some of the perovskite and perovskite-related substrates that are available commercially (*below* the number line).

stimulated the production of many perovskite single crystals (45–54) to diameters up to four inches as well as spawned a number of new perovskite and perovskite-related substrates (55–58). These single-crystal perovskite and perovskite-related substrates include $YAlO_3$ (50), $LaSrAlO_4$ (55), $LaAlO_3$ (52, 54), $LaSrGaO_4$ (56), $NdGaO_3$ (46, 51), $(LaAlO_3)_{0.29}$-$(Sr_{1/2}Al_{1/2}TaO_3)_{0.71}$ (LSAT) (57), $LaGaO_3$ (45), $SrTiO_3$, and $KTaO_3$ (48); many are produced with structural perfection rivaling that of conventional semiconductors. **Figure 2** shows the pseudotetragonal or pseudocubic *a*-axis lattice spacings offered by these commercial substrates, together with the corresponding lattice spacings of several ferroelectrics. As can be seen in **Figure 2**, the lattice constants of the available perovskite substrates tend to be smaller than many of the ferroelectric materials of current interest. This is because most of the commercially available perovskite substrates were developed for high-temperature superconductors, which typically have lattice constants in the 3.8–3.9-Å range. Rare-earth scandate (*Re*ScO_3) substrates have been recently developed with the larger lattice constants of ferroelectric perovskites in mind (59–61).

In addition to appropriate substrate single crystals, a method to prepare substrates with a specific chemical termination of the surface is a prerequisite for atomic-layer-controlled thin film growth of epitaxial heterostructures. For example, chemical-mechanically polished (100) $SrTiO_3$ substrates display a mixture of SrO- and TiO_2-terminated surfaces. Kawasaki et al. (62) showed that an NH_4F-buffered HF solution with controlled pH enables etching of the more basic SrO layer and leaves a completely TiO_2-terminated surface on the substrate (62). Koster et al. (63) have further perfected this method of preparing a TiO_2-terminated (100) $SrTiO_3$ surface. SrO-terminated (100) $SrTiO_3$ substrates can also be prepared (64). A means to prepare defect-free surfaces with controlled termination has also been developed for (110) $LaAlO_3$[3] (65; D.H.A. Blank, private communication), (110) $NdGaO_3$[3] (65; D.H.A. Blank, private communication), (100) LSAT (65), (100) $KTaO_3$ (66), and (110) $DyScO_3$ substrates (D.H.A. Blank, private communication).[3]

THEORY AND SIMULATION OF THE EFFECTS OF STRAIN ON FERROELECTRICS

The theoretical approaches developed to understand and model ferroelectric thin films cover essentially the entire spectrum of methods that have been developed for condensed matter systems. In approximate order of increasing required input of external information and increasing ability to treat larger system sizes, these include first-principles calculations that determine electronic structure by solving Schrödinger's equation at zero temperature, effective Hamiltonian methods that parameterize the Hamiltonian in a way such that finite temperature calculations can be performed, molecular dynamics simulations utilizing interatomic potentials based on parameters that have been fit to either experimentally or first-principles-derived results, phenomenological models based on Ginzburg-Landau theory that capture the salient features of the thermodynamic free energy for a particular set of boundary conditions as a function of internal and external variables, and phase-field and finite-element models that are able to treat truly complex microstructures.

First-principles calculations allow the prediction of atomic arrangements and polarization-related properties without input of experimental information. Rapid progress over the past 15 years in algorithms—particularly ultrasoft pseudopotentials, efficient implementations (including VASP, Abinit, PWscf, SIESTA, and Wien2K), the modern theory of polarization, and density functional perturbation theory—has been key to making these methods into useful tools for the prediction of the properties of ferroelectric thin films and superlattices, increasing the size and complexity of the structures that can be accurately investigated (67). At the same time, the length scales of control of atomic ordering achievable in ferroelectric heterostructures have been decreasing (34, 68–74), enabling the same systems to be studied both experimentally and from first principles (75). To be more precise, first-principles density-functional-theory methods can handle supercells of up to approximately 100 atoms, allowing calculations for perovskite superlattices with a period of up to 20 perovskite cells and slab calculations for surfaces that include adequate bulk and vacuum layers. At longer time- and length scales, a multiscale approach can be implemented. Interatomic potentials and effective Hamiltonians constructed from first-principles input can be used for supercells with up to several thousand atoms (76–79). Phenomenological approaches that reach macroscopic continuum scales, such as Landau-Devonshire theory, can draw on first-principles results to determine theoretical parameters and thus can extend accurate phenomenological analysis to regimes of high strain and electric fields for which experimental information is not available (80). Furthermore,

---

[3] The Miller indices given for the surfaces of $LaAlO_3$, $NdGaO_3$, and $DyScO_3$ reflect their noncubic symmetry at room temperature. In pseudocubic notation these are all {100} pseudocubic surfaces.

if the phase-field method based on time-dependent Ginzburg-Landau equations is employed, it is possible to predict the domain structures and properties of ferroelectric thin films and their dependence on temperature, substrate constraint, electrical boundary conditions (31–36), thickness, and inhomogeneous defect distributions (81).

Strain-Phase Diagrams of Single-Layer Ferroelectric Thin Films

The effects of biaxial strain and temperature on ferroelectric transitions and domain structures have been theoretically studied for a number of ferroelectrics. These include $(001)_p$-oriented $PbTiO_3$ (15, 16, 18, 19), $BaTiO_3$ (15, 21, 22, 78), and $Pb(Zr_xTi_{1-x})O_3$ (81a, 81b) as well as $(001)_p$ $SrTiO_3$ (17, 20, 21), which is not normally ferroelectric but can become ferroelectric when strained; the subscript p refers to the pseudocubic index. The orientation relationship of an $(001)_p$-oriented, biaxially strained ferroelectric perovskite film on an $(001)_p$ perovskite substrate is shown schematically in **Figure 1**. Strain-phase diagrams for these thin films, which graphically display the ferroelectric phase transition temperatures and domain structures as a function of strain, have been constructed via thermodynamic analysis and phase-field simulations.

The initial versions of strain-phase diagrams for $PbTiO_3$ and $BaTiO_3$ were generated via thermodynamic analyses by assuming a single, homogeneous domain state for all possible ferroelectric phases in a thin film. The most stable phase for a given temperature and strain was determined by comparing the energies of all possible ferroelectric phases as well as the parent paraelectric phase (15). Because under a given temperature and strain a ferroelectric state in a thin film almost always contains more than one type of domain, improved versions of strain-phase diagrams were obtained by allowing each ferroelectric phase to form simple two-dimensional, two-domain ferroelectric states with a priori domain-wall orientations. The most stable ferroelectric state was then determined by comparing the energies of single-domain or two-domain states of all possible ferroelectric phases (16). To take into account the full three-dimensional domain structures that contain all possible types of domains, phase-field models have been developed to predict strain-phase diagrams (19, 81). Phase-field models, although computationally more expensive, do not make a priori assumptions on the possible ferroelectric phases and domain structures that might appear under a given temperature and substrate constraint. The domain structures in a phase-field model are predicted by annealing a quenched paraelectric state with a fixed substrate constraint and temperature.

Different levels of approximations and assumptions for the ferroelectric phases, e.g., single-domain states or two-dimensional two-domain states in thermodynamic analysis, or full three-dimensional multidomain states in phase-field simulations, have been utilized in theoretical investigations aimed at understanding equilibrium strain-phase diagrams of ferroelectric films. Depending on the approximations and assumptions used, quantitatively and often qualitatively different results are obtained as the level of sophistication is increased for treating the energetics of what is generally a complex three-dimensional microstructure. **Figure 3** shows examples of strain-phase diagrams for $(001)_p$-oriented $PbTiO_3$ films from thermodynamic analysis and

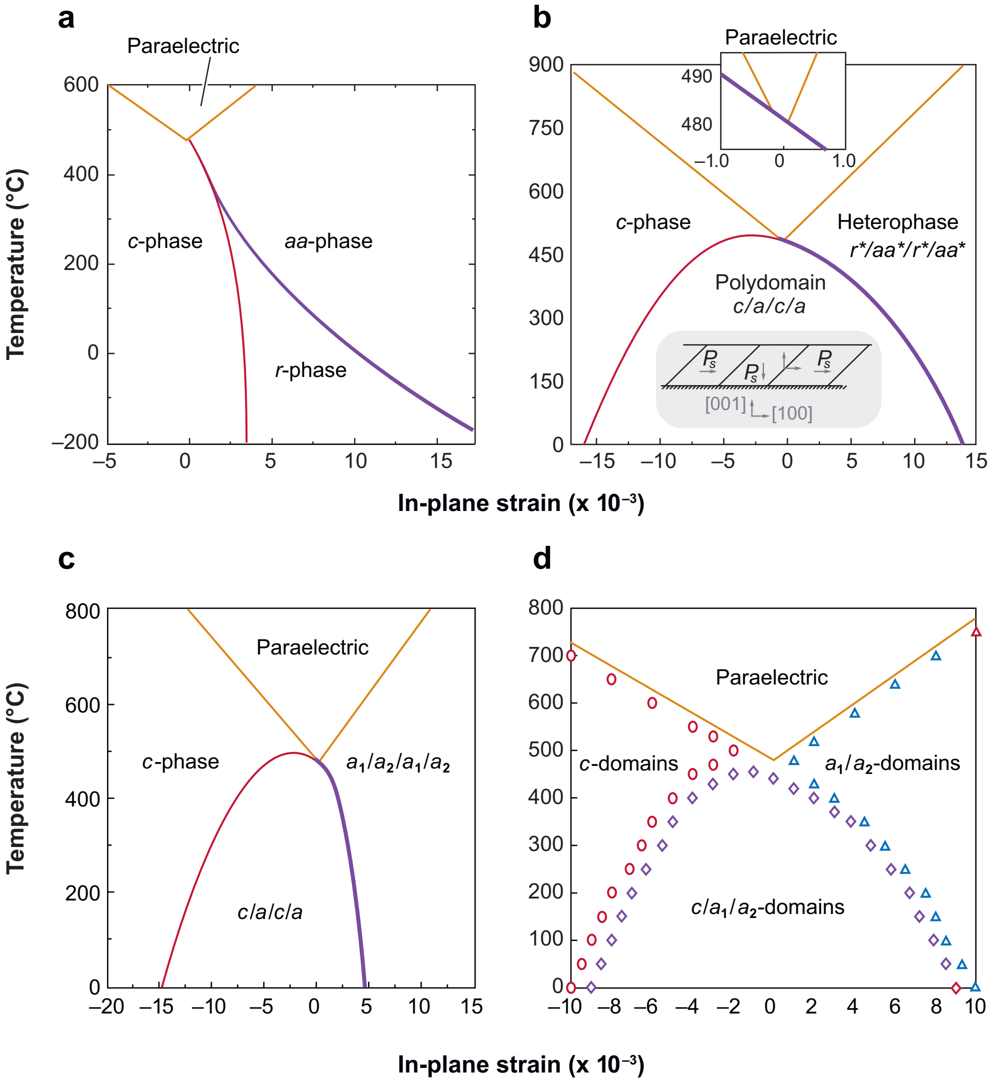

Figure 3

Four strain-phase diagrams of $(001)_p$-oriented $PbTiO_3$ calculated using thermodynamic analysis or phase-field simulations and different assumptions of the ferroelectric domain states. (*a*) Single domain for all ferroelectric states (reprinted from Reference 15, with permission; copyright 1998 by the American Physical Society). (*b*) Either single- or double-domain states with domain-wall orientations restricted to be 45° from the film/substrate interface (reprinted from Reference 16, with permission; copyright 2000 by the American Physical Society). (*c*) Single- or double-domain states with domain-wall orientations restricted to be either 45° or 90° from the film/substrate interface (reprinted from Reference 18, with permission; copyright 2001 by the American Physical Society). (*d*) From three-dimensional phase-field simulations that automatically predict the possible multidomain states without assuming the domain-wall orientations (reprinted from Reference 81, with permission; copyright 2002, Elsevier).

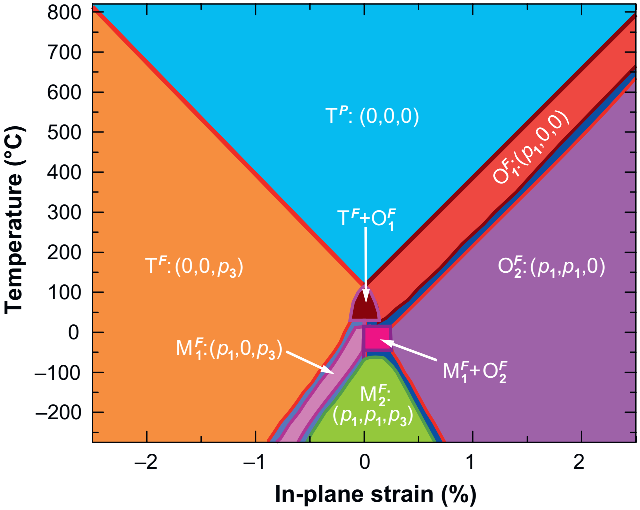

Figure 4

The strain-phase diagram of $(001)_p$-oriented $BaTiO_3$ obtained from phase-field simulations. The letters T, O, and M used in the phase notations indicate tetragonal, orthorhombic, and monoclinic crystallographic symmetries, respectively, under a constraint. The paraelectric and ferroelectric natures of the phases are revealed by the superscripts *P* and *F*, respectively. $M_1^F + O_2^F$ implies a mixture of M_1^F and O_2^F phases. The components of the polarization vector *P* corresponding to the phases (along the crystallographic directions of pseudocubic $BaTiO_3$) are indicated within the parentheses following the phase notation (adapted from Reference 22, with permission; copyright 2006, American Institute of Physics).

phase-field simulations, indicating clear differences for different approximations and assumptions about the domain configurations. For $BaTiO_3$, multiple ferroelectric phase transitions are involved, and the strain-phase diagram is more complicated than that of $PbTiO_3$. **Figure 4** is an example of a strain-phase diagram for $BaTiO_3$ that was obtained by phase-field simulations (22). At low temperatures, unstrained bulk $SrTiO_3$ undergoes a structural transition involving the rotation of oxygen octahedra. **Figure 5** gives the strain-phase diagram derived from thermodynamic analysis, assuming a single-domain state for $SrTiO_3$ thin films; this figure indicates room-temperature ferroelectricity of a $SrTiO_3$ with sufficiently large tensile strains, which is otherwise nonferroelectric.

Quantitative predictions by either thermodynamic analysis or phase-field simulations are possible only for ferroelectrics whose properties have been sufficiently characterized to determine their bulk thermodynamic properties. Recently, with the assumption of a single-domain state for the ferroelectric phases, Diéguez et al. (78) demonstrated that it is also possible to obtain strain-phase diagrams directly through first-principles methods. **Figure 6** shows an example for $(001)_p$ $BaTiO_3$ (78). A future direction will be to combine first-principles calculations and phase-field simulations, making it possible to predict strain-phase diagrams for a wide variety of ferroelectric materials while taking full three-dimensional domain structures into account. These theoretical predictions, represented in the form of strain diagrams in **Figures 3–6**,

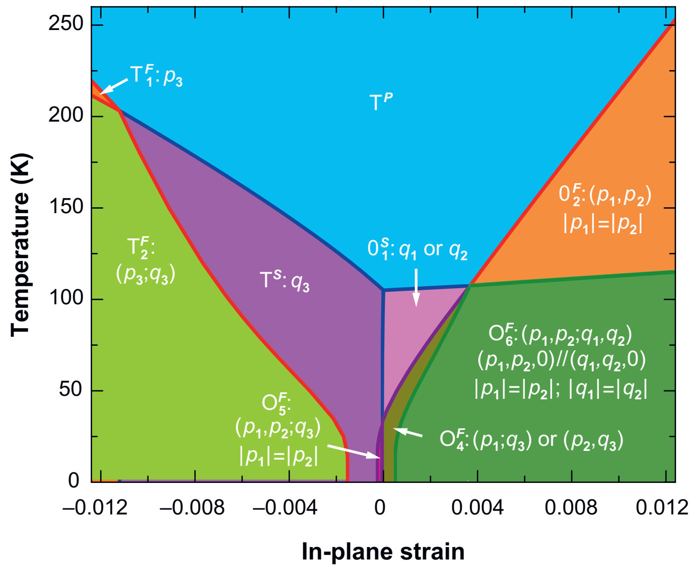

Figure 5

The strain-phase diagram of (001)$_p$-oriented SrTiO$_3$ calculated assuming a single-domain state for all structural and ferroelectric phases (adapted from Reference 23, with permission; copyright 2006 by the American Physical Society). Nomenclature identical to that of **Figure 4** is used to describe the crystallographic symmetry of the phases and order parameters. This diagram has only a minor difference from that presented in Reference 17.

can serve as guides to experimentalists interested in enhancing the properties of ferroelectric thin films via strain engineering.

Domains in Strained Ferroelectric Films

A common feature of all ferroelectric crystals is the formation of domain structures when a paraelectric phase is cooled through the ferroelectric transition temperature.

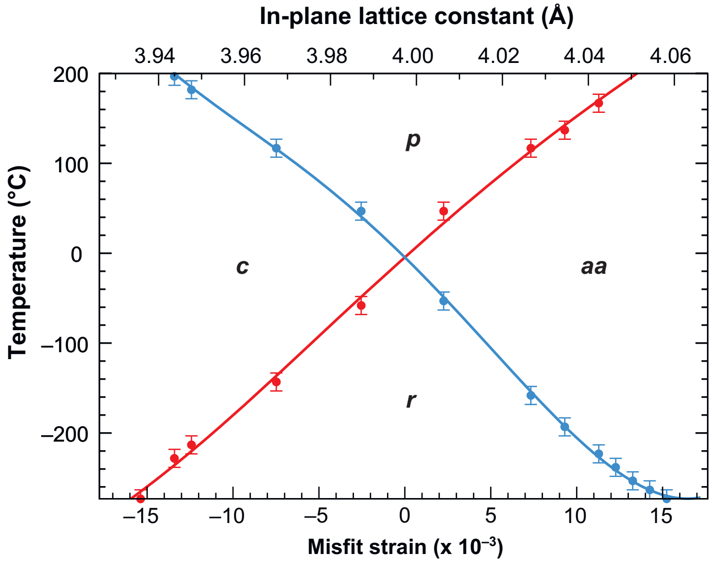

Figure 6

The strain-phase diagram of (001)$_p$-oriented BaTiO$_3$ calculated from first principles. *p*, paraelectric phase; *c*, out-of-plane tetragonal phase; *aa*, orthorhombic phase with polarization components $p_x = p_y$ and $p_z = 0$; *r*, a ferroelectric phase with $p_x = p_y \neq p_z \neq 0$ (reprinted from Reference 78, with permission; copyright 2004 by the American Physical Society).

Each individual domain is a micro/nanoscale region with uniform electrical polarization. The type of domain structures formed in a thin film depends critically on the crystallographic relationship between the paraelectric and ferroelectric phases, the film orientation, the substrate constraint, electrical boundary conditions on the surface and at the film/substrate interface, and the inhomogeneous distribution of defects within a thin film. With the theoretical tools available, it is now possible to study systems that develop domain structures under boundary conditions realized in experimental configurations. For example, the rich phase diagram of $PbTiO_3$ films on an $SrTiO_3$ substrate (29) (shown in **Figure 12**, below) contains uniform states and stripe domains of different widths as thickness and temperature vary. First-principles calculations of the $PbTiO_3/SrTiO_3$ interface, the free $PbTiO_3$ surface, and the domain-wall energies in the film geometry can establish the boundary conditions and surface energy terms for a continuum treatment of the domain structures such as thermodynamic analysis of domain stability or phase-field simulations of domain formation. **Figure 7** shows examples of domain structures in $BaTiO_3$ thin films under three different substrate constraints and temperatures (22). Dislocations often exist in thin films, and their density depends on the lattice mismatch and film thickness. It is possible to incorporate both static and mobile interfacial dislocations into

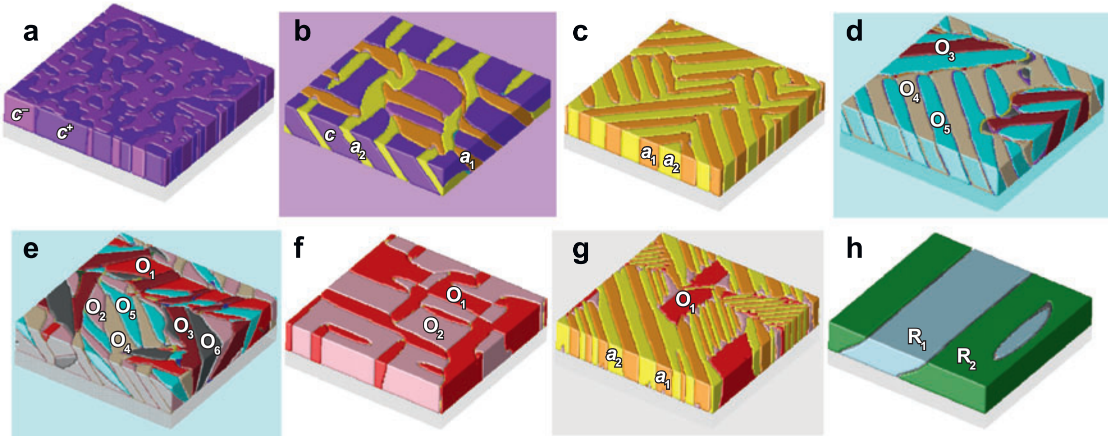

Figure 7

Domain morphologies in $BaTiO_3$ films as a function of temperature (T) and substrate constraint strain (ε_s). Domain definitions: a_1: $(P_1,0,0)$; a_2: $(0,P_1,0)$; c: $(0,0,P_3)$; R_1: $(-P_1,-P_1,P_3)$; R_2: $(P_1,-P_1,P_3)$; O_1: $(P_1,P_1,0)$; O_2: $(P_1,-P_1,0)$; O_3: $(P_1,0,P_3)$; O_4: $(P_1,0,-P_3)$; O_5: $(0,P_1,P_3)$; O_6: $(0,P_1,-P_3)$. (*a*) Tetragonal *c* domains separated by 180° domain walls at $T = 25°C$ and $\varepsilon_s = -1.0\%$. (*b*) Three variants of distorted tetragonal domains, $c/a_1/a_2$, at $T = 75°C$ and $\varepsilon_s = 0.0$. (*c*) Two variants of in-plane distorted tetragonal domains, a_1/a_2, separated by 90° domain walls (twin walls) at $T = 50°C$ and $\varepsilon_s = 0.2\%$. (*d*) Three variants of orthorhombic domains, $O_3/O_4/O_5$, at $T = -25°C$ and $\varepsilon_s = -0.05\%$. (*e*) Six variants of orthorhombic domains O_{1-6} at $T = -25°C$ and $\varepsilon_s = 0.1\%$. (*f*) Two variants of O_1/O_2 domains at $T = 25°C$ and $\varepsilon_s = 1.0\%$. (*g*) Mixture of tetragonal a_1/a_2 domains and orthorhombic O_1/O_2 domains at $T = 25°C$ and $\varepsilon_s = 0.25\%$. (*h*) Rhombohedral R_1/R_2 domains at $T = -100°C$ and $\varepsilon_s = 0.1\%$ (reprinted from Reference 22, with permission; copyright 2006, American Institute of Physics).

a phase-field model and study the interactions between dislocations and domains in ferroelectric thin films. Fundamental understanding achieved through these theoretical tools can then suggest new combinations of materials, substrates, and interface buffer layers to achieve the stabilization of desired phases and domain structures.

SPM: scanning probe microscope

PFM: piezo-force microscopy

TEM: transmission electron microscopy

XPD: X-ray photoelectron diffraction

CHARACTERIZATION METHODS RELEVANT TO STUDYING STRAINED FERROELECTRIC THIN FILMS

In recent years, scanning probe microscopy has emerged as one of the key techniques for the study of ferroelectric materials. Using a metallic scanning probe microscope (SPM) tip as an electrode to generate a local switching field allows precise and reversible control of ferroelectric polarization at the nanoscale. The polarization state itself can be directly probed at the same scales by using the SPM tip to measure the local piezoelectric response of the film to a small applied oscillating voltage (piezo-force microscopy, or PFM; see below), its local nonlinear dielectric permittivity (scanning nonlinear dielectric microscopy), the voltage derivative of the capacitance between the tip and the surface (scanning capacitance microscopy), or the electrostatic force gradient and effective surface potential (scanning surface potential microscopy) of stray electric fields above the ferroelectric film due to the presence of surface charge. Local studies of the optical properties of the surface, using near-field optical microscopy, can also provide information on the ferroelectric polarization. A detailed review of these different methods may be found elsewhere (82).

Transmission electron microscopy (TEM) plays an important role in establishing the limits to which ferroelectric thin films and superlattices can be strained. As the key approach for imaging interface structure and extended defects in thin films, it has been essential in experimentally determining the critical thickness for epitaxial strain relaxation by dislocation introduction and in understanding the resulting dislocation arrays and their impact on properties (40, 41, 44, 83–86).

As the polarization of a ferroelectric is directly related to the noncentric positions of atoms in the unit cell, significant ferroelastic strains are frequently developed as the phase transition occurs. Methods that provide direct information on structure therefore can be used to probe ferroelectricity. Laboratory-source experiments can determine the strain in ferroelectric films with thicknesses down to a few unit cells (87). This strain information can be analyzed in terms of an underlying polarization through an understanding of electrostriction. Researchers have developed synchrotron X-ray scattering techniques that make use of the extremely high X-ray brilliance that is provided at synchrotron-light-source user facilities (88). Such techniques enable in situ measurements as a function of, for instance, temperature (89) or electric field (90, 91) and detailed structural analysis beyond average lattice parameter measurements by the measurement of crystal truncation rod intensities well away from Bragg peaks (92). These approaches allow atomic positions as a function of depth within a film to be determined with unit-cell precision and therefore give insight into the structural gradients at surfaces and interfaces.

Another interesting approach to probe ferroelectricity in ultrathin films is to use X-ray photoelectron diffraction (XPD) (93), a technique applied mostly to studies

MORE ON ELECTROSTRICTION

Electrostriction is elastic strain ε induced by the application of an electric field or by spontaneous or induced polarization, $\boldsymbol{P}$, that is quadratic in nature ($\varepsilon \propto \boldsymbol{P}^2$) and thus produces a strain that is independent of the sign of the applied field. Piezoelectric properties in ferroelectric materials can be formally derived in terms of the temperature-independent electrostrictive properties of the material (that do not change across the paraelectric-to-ferroelectric phase transition) and the temperature-dependent polarization in the ferroelectric state. Thus, generally the simplest fundamental description of the electromechanical properties of ferroelectrics is based on electrostriction.

of the orientation of adsorbed molecules, surface segregation, and interdiffusion at interfaces. This technique is element specific, surface sensitive (has 20–30-Å probing depth, depending on the photon energy), and yields information on the atomic structure of the surface layer. Because of the chemical sensitivity of photoemission, a given atom type can be chosen by the selection of one of the atom's core levels. The local geometry around the selected atom can then be probed by performing intensity-versus-emission-angle scans of a chosen photoemission line. The resolution of this technique is sufficient to directly probe the intracell atomic displacements associated with ferroelectricity and to measure the material tetragonality (94).

XRD: X-ray diffraction

The power of XPD is revealed by recent measurements on monodomain epitaxial $(001)_p$ $PbTiO_3$ films to determine the tetragonality of the $PbTiO_3$ films as thin as one unit cell at room temperature (94). **Figure 8** presents the results. Both XPD and high-resolution X-ray diffraction (XRD) measurements (87) point to a systematic decrease of the *c*-axis lattice parameter, with decreasing film thickness below 200 Å. Because

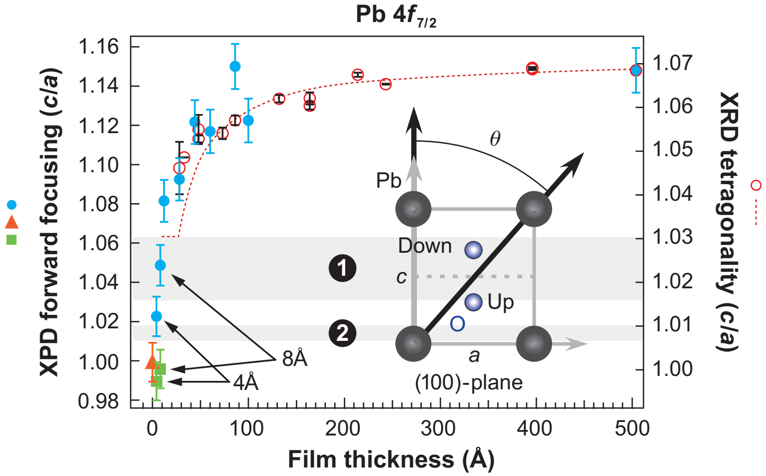

Figure 8

Evolution of the *c/a* ratio at room temperature with film thickness for commensurate $(001)_p$-oriented $PbTiO_3$ films grown on Nb-doped (100) $SrTiO_3$ substrates. XPD results (*left scale*, *blue circles*) are compared with XRD results (*red circles*, *right scale*) (reprinted from Reference 94, with permission; copyright 2006 by the American Physical Society).

of the strong strain polarization coupling in $PbTiO_3$, the material tetragonality is strongly influenced by the polarization. The evolution of c/a is therefore taken as a signature of the progressive reduction of $\boldsymbol{P}$ and suppression of ferroelectricity in ultrathin films. This decrease in polarization can be explained by a residual unscreened depolarizing field, as predicted in Reference 33.

The good agreement between the XPD (94), which is very surface sensitive, and the XRD data (87), which average over the whole film, implies that the polarization evolves at the surface in the same way as in the interior of the film and that there is no thick paraelectric dead layer at the surface. The XPD tetragonality measurement also shows a continuous decrease of tetragonality down to a thickness of one unit cell. The tetragonality of a one-unit-cell-thick paraelectric film was obtained from ab initio calculations (94). The value obtained is in good agreement with the experimental one, suggesting that the one-unit-cell-thick $PbTiO_3$ film is paraelectric. The calculations also show that at this thickness the interlayer atomic distances are strongly affected by surface relaxation and rumpling (94).

XPD was also used to directly probe the intracell atomic displacements associated with ferroelectricity in $PbTiO_3$ films as thin as 20 Å (the experimental limit when O is chosen as the emitter, a limit linked to the presence of O in the substrate). The results unambiguously demonstrate that the O atoms have a noncentrosymmetric position in the Pb cage in films down to this thickness (94). The XPD data combined with ab initio calculations suggest that $PbTiO_3$ films as thin as three unit cells are still ferroelectric. For films with thicknesses of one or two unit cells, the asymmetry of the atomic relaxations at the free surface and at the substrate interface makes the film naturally polar. Switching of this polar distortion is, however, unlikely.

A technique that is finding increasing application to ferroelectric thin films is Raman spectroscopy. The ferroelectric phase transition is intimately related to specific phonon modes whose frequency depends on temperature. These excitations can in turn be observed via Raman scattering by the use of heterostructures that provide high selectivity for a ferroelectric film over its underlying substrate, for instance by having an interposed Raman-inactive electrode that screens the substrate. Mode structure has been tracked in films with thicknesses of the order of a few hundred nanometers. Even though this is not strictly thin, given recent results on ferroelectricity in films, it has allowed researchers to observe changes in mode structure that advance our understanding of the ferroelectric phase transition in constrained geometries (95). Alternatively, ultraviolet (UV) illumination limits penetration into a heterostructure and thus enhances signal from a film; therefore, UV illumination has become a promising method for tracking symmetry and phase behavior in much thinner ferroelectric thin films (tens of nanometers) and superlattices (74).

T_C has been determined on strained thin films through the use of several experimental methods. The conventional method of measuring a hysteresis loop is problematic when the electrical leakage current is high, e.g., for extremely thin films in which currents due to electron tunneling are high or at elevated temperatures at which significant ionic conductivity can occur. The conventional method also requires electrodes, which alter the electrical boundary conditions and can impose experimental complications. For sufficiently thick ferroelectric films and superlattices,

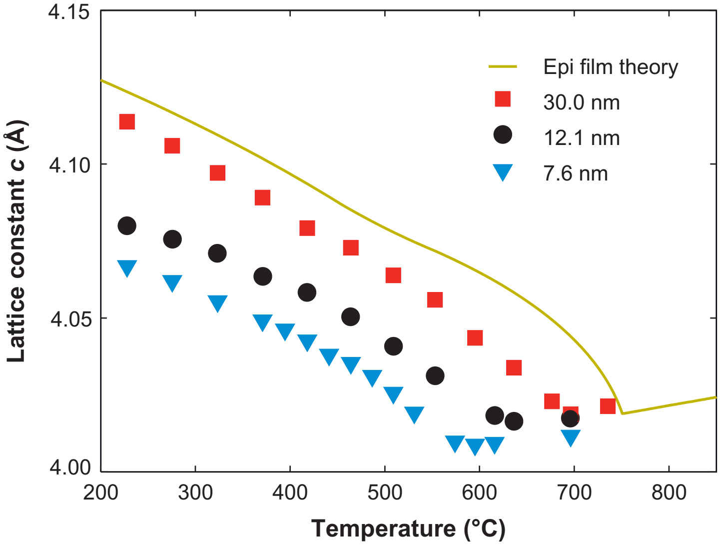

Figure 9

Temperature dependence of the out-of-plane lattice parameter of a coherent $(001)_p$-oriented $PbTiO_3$ film grown by metalorganic chemical vapor deposition (MOCVD) on (100) $SrTiO_3$ substrates. The change in slope at high-temperature signals the paraelectric-to-ferroelectric phase transition, i.e., T_C. (Data taken at the Advanced Photon Source, beamline 12-ID-D, via methods described in Reference 29.)

UV Raman can be used to determine T_C (74). Two methods that at high temperatures are applicable to extremely thin ferroelectric films have become popular. One method involves measuring the temperature dependence of the out-of-plane lattice parameter of the strained film. A kink in the out-of-plane lattice parameter occurs at T_C, as is shown in **Figure 9** for a coherent $PbTiO_3$ film. Such kinks at T_C have been observed in a number of coherently strained ferroelectric films (21, 24, 29) and are expected from theory (21, 29, 96). A second method is to use second harmonic generation (SHG). **Figure 10** shows the results of an SHG measurement on a coherently strained $BaTiO_3$ film. Only materials that lack inversion symmetry exhibit an SHG signal. All ferroelectrics must lack inversion symmetry, but there are many materials that lack inversion symmetry and are not ferroelectric. This makes SHG a necessary but insufficient probe for ferroelectricity. A better test for ferroelectricity with SHG is to monitor changes in the symmetry of the SHG response that occur when external electric fields are applied; such changes imply the presence and rearrangement of ferroelectric domains (97, 98).

EXPERIMENTAL RESULTS ON SINGLE-LAYER STRAINED FERROELECTRIC FILMS

Strained $(001)_p$ $SrTiO_3$ Films

SHG: second harmonic generation

The strain-phase diagrams in **Figures 3–6** imply that ferroelectrics can be very sensitive to strain. These predictions imply that a biaxial tensile strain of order 1% will shift the T_C of $SrTiO_3$, a material that normally is not ferroelectric at any temperature, to the vicinity of room temperature. Comparable shifts in transition temperature, roughly 300 K per percent biaxial strain, are expected for $PbTiO_3$ and

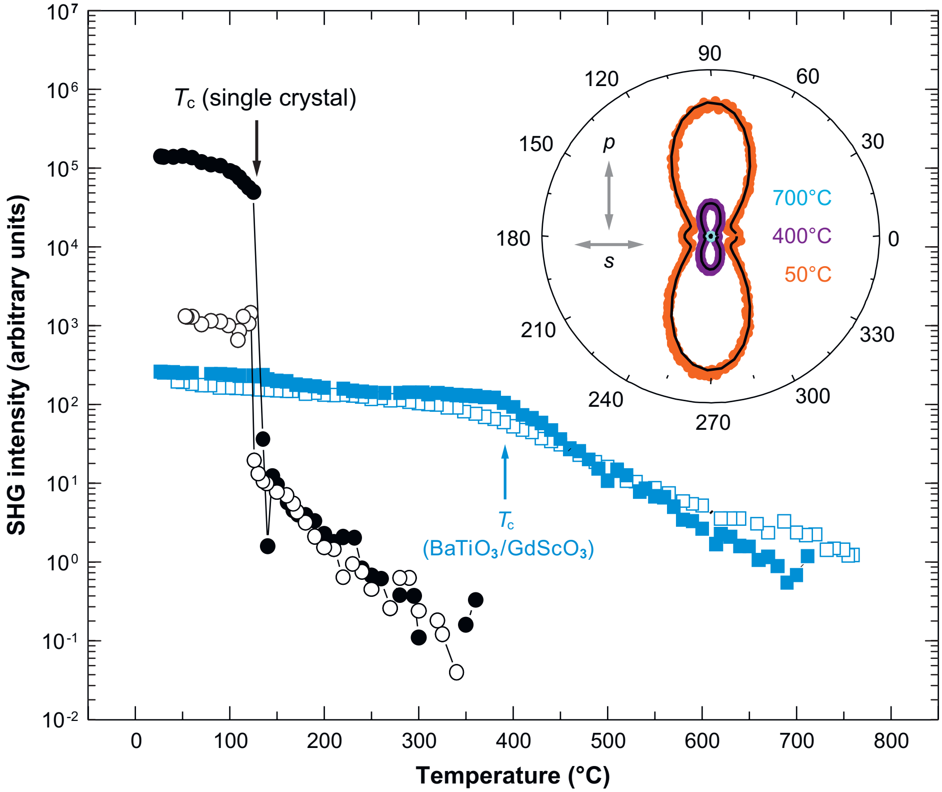

Figure 10

Optical second harmonic generation (SHG) signals from a coherent 1000-Å-thick $(001)_p$-oriented $BaTiO_3$ film grown by molecular-beam epitaxy (MBE) on a (110) $GdScO_3$ substrate. The inset shows polar plots of SHG intensity (radius) versus fundamental polarization (azimuth). In the inset, circles represent data from experiments, and solid lines represent theory. The kink in the SHG-versus-temperature plot occurs at the same temperature as does the kink in the out-of-plane lattice parameter versus temperature (shown in **Figure 13**), i.e., at T_C (from Reference 21).

$BaTiO_3$. These predictions have been borne out by experiments on strained $SrTiO_3$ (**Figure 11**) (20), $PbTiO_3$ (**Figures 9** and **12**) (29, 35), and $BaTiO_3$ (**Figure 13**) films (21); large strain effects of comparable magnitude were observed earlier in $KTaO_3/KNbO_3$ (24, 26), $SrTiO_3/SrZrO_3$ (25), and $SrTiO_3/BaZrO_3$ superlattices (30) and strained $(Ba,Sr)TiO_3$ films (27, 28). These strained $SrTiO_3$ films grown on (110) $DyScO_3$ substrates show a tunability of the dielectric constant at room temperature of 82% at 10 GHz (20) and dielectric constant maxima near 20,000 at 500 Hz (99).

An example of the structural perfection possible in strained ferroelectric films is shown in **Figure 14**, in which the rocking-curve full width at half maximum (FWHM) of (*a*) strained $SrTiO_3$ films and typical commercial $SrTiO_3$ single crystals and (*b*) strained $BaTiO_3$ films and commercial $BaTiO_3$ single crystals are compared. With

FWHM: full width at half maximum

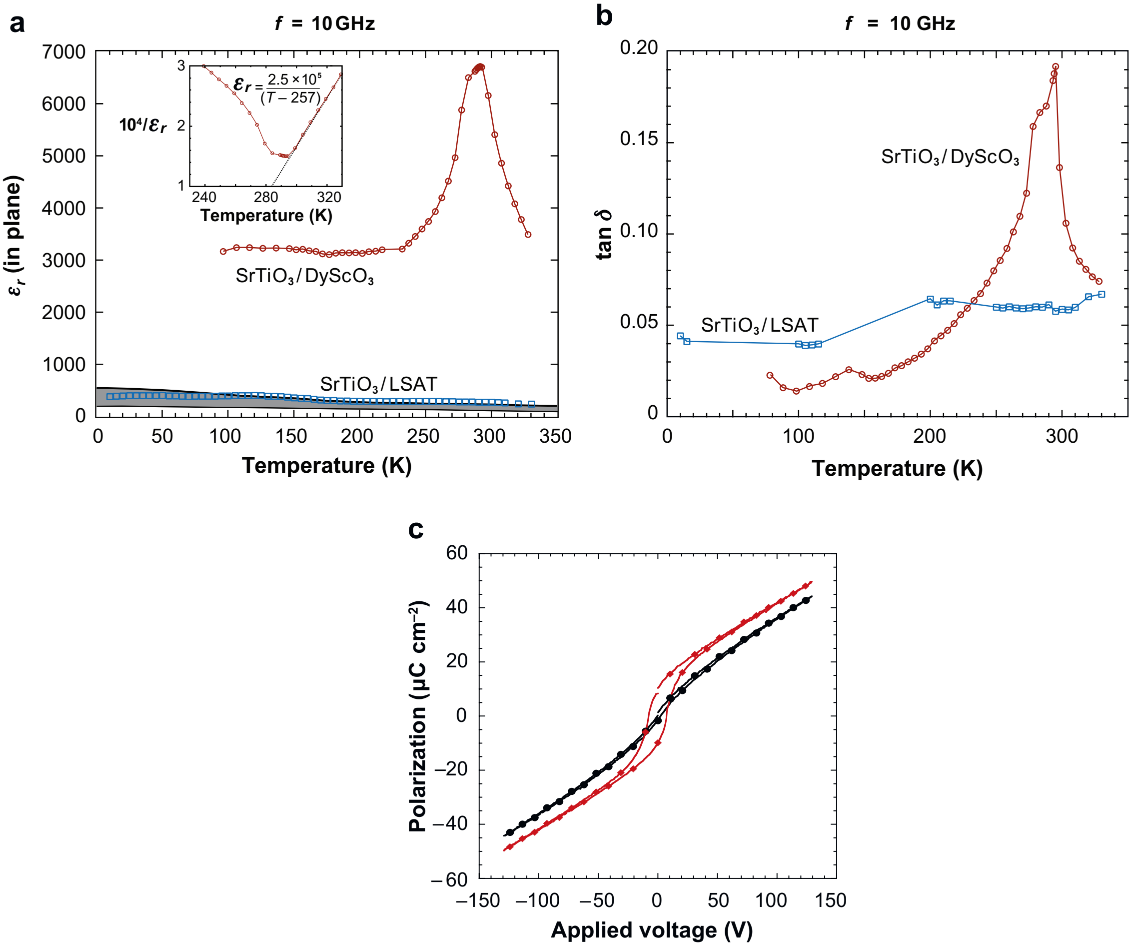

Figure 11

In-plane dielectric constant (ε_r) and dielectric loss (tan δ) in strained epitaxial $(001)_p$-oriented $SrTiO_3$ films as a function of temperature at a measurement frequency, *f* of 10 GHz. Panels *a* and *b* contrast in-plane ε_r and tan δ, respectively, of 500-Å-thick $SrTiO_3$/(110) $DyScO_3$ and $SrTiO_3$/(100) $(LaAlO_3)_{0.29}$-$(Sr_{1/2}Al_{1/2}TaO_3)_{0.71}$ (LSAT) epitaxial films grown by molecular-beam epitaxy (MBE). These nearly coherent films are under $\varepsilon_s = +0.9\%$ biaxial tensile and $\varepsilon_s = -0.9\%$ compressive strain, respectively. The simultaneous peak in ε_r and tan δ indicates that the T_C of $(001)_p$ $SrTiO_3$ under biaxial tension of $\varepsilon_s = +0.9\%$ is ~293 K. The inset in *a* shows a Curie-Weiss fit to $1/\varepsilon_r$. The shaded region in *a* corresponds to the expected value of the in-plane ε_r for a $(001)_p$ $SrTiO_3$ film coherently strained to LSAT ($\varepsilon_s = -0.9\%$), on the basis of thermodynamic analysis and the range of relevant reported property coefficients for $SrTiO_3$. Subpanels *a* and *b* are from Reference 20. (*c*) Hysteresis loops measured at room temperature (*black*) and in liquid nitrogen at 77 K (*red*). The large slope is due to uncorrected parasitic capacitance. Panel *c* is reprinted from Reference 99, with permission; copyright 2006, American Institute of Physics.

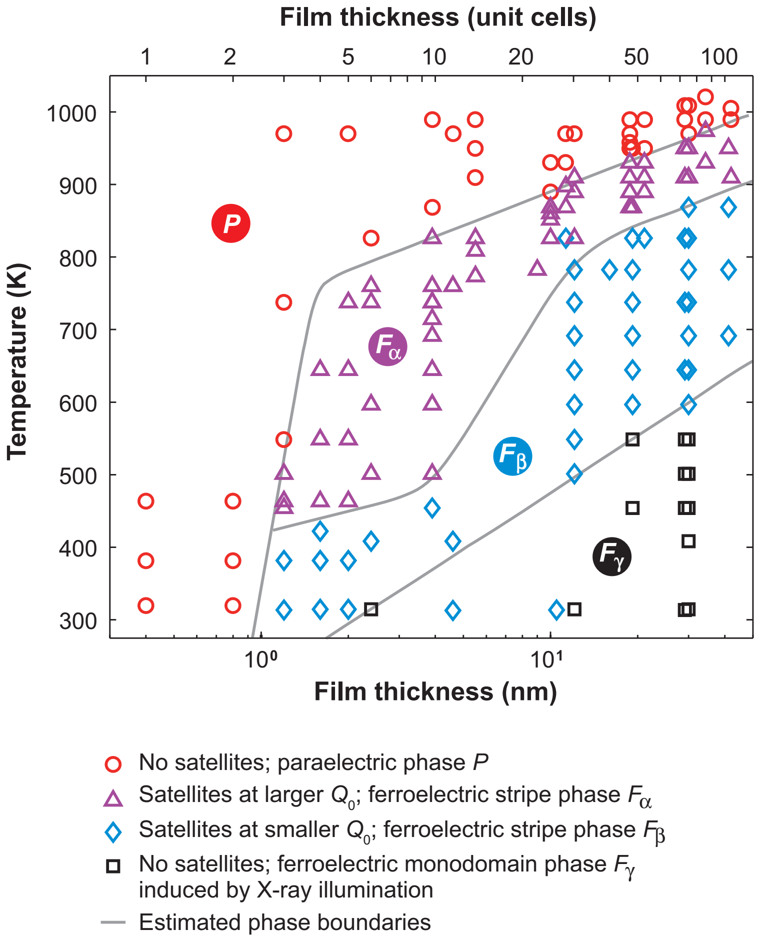

Figure 12

Phase diagram of coherent epitaxial $(001)_p$ $PbTiO_3$ thin films on (100) $SrTiO_3$, determined through a combination of lattice parameter measurements for thicker films and analysis of diffuse scattering. Adapted from online supporting material for Reference 35.

rocking-curve widths as narrow as 7 arc s (99), these epitaxial $SrTiO_3/DyScO_3$ films not only have the highest structural quality ever reported in heteroepitaxial films of any oxide grown by any technique but even have better structural perfection than do $SrTiO_3$ single crystals (100, 101). Similarly, the growth of $BaTiO_3$ films on $GdScO_3$ substrates has achieved films with narrower rocking curves than do $BaTiO_3$ single crystals (21). This structural perfection arises from the excellent structural perfection of commercially available $Re$$ScO_3$ substrates (61); they are grown by the Czochralski method, which is not applicable to either $SrTiO_3$ or $BaTiO_3$. The rocking-curve widths of these strained films are within instrumental error identical to those of the substrates upon which they are grown.

Strained $(001)_p$ $PbTiO_3$ and $(001)_p$ $Pb(Zr_xTi_{1-x})O_3$ Films

Figure 12 shows the thickness dependence of fully coherent $(001)_p$ $PbTiO_3$ films grown on (100) $SrTiO_3$. In the absence of any thickness dependence, the nearly

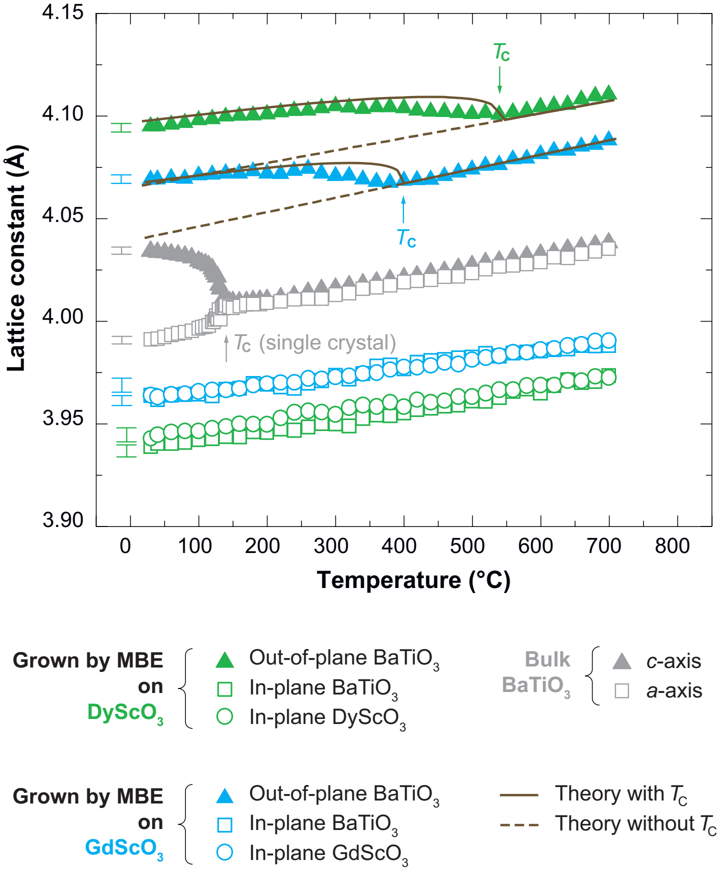

Figure 13

Temperature dependence of the lattice parameters of single-crystal $BaTiO_3$ and strained $BaTiO_3$ thin films grown by MBE on $DyScO_3$ and $GdScO_3$ substrates. The in-plane and out-of-plane lattice constants of the $BaTiO_3$ thin films and underlying substrates are shown. The change in slope at high temperature signals a phase transition. The error bars (± standard deviation) of the measured lattice constants are shown at the left edge of each curve. The measured values of the out-of-plane spacing of biaxially strained $BaTiO_3$ are compared with theoretical predictions with (*solid line*) and without (*dashed line*) a ferroelectric transition. Figure from Reference 21.

1% biaxial compressive strain of this system is predicted to increase T_C by approximately 260°C for perfectly coherent $(001)_p$ $PbTiO_3/SrTiO_3$. This enhancement is approached in the thicker films, but for thin films a clear reduction of T_C is evident. This result shows that in addition to strain and electrical boundary conditions (31–36) size also has a dramatic influence on ferroelectric properties (33–35, 67, 103).

A system that has been extensively studied experimentally is $(001)_p$-oriented $Pb(Zr_xTi_{1-x})O_3$ deposited onto (100) $SrTiO_3$, with x chosen from within the tetragonal region of the phase diagram, $0 \leq x \leq 0.52$ (34, 103–105). Several reasons account for the popularity of the $(001)_p$ $Pb(Zr_xTi_{1-x})O_3$ system. First, it is possible to synthesize very-high-quality epitaxial $(001)_p$ $Pb(Zr_xTi_{1-x})O_3$ films on (100) $SrTiO_3$ substrates with the $Pb(Zr_xTi_{1-x})O_3$ film under biaxial compressive strain. This tends to force the ferroelectric polarization to be out of the substrate plane, which is the orientation that is most straightforward to probe by most methods. Furthermore, the $Pb(Zr_xTi_{1-x})O_3$ ferroelectric phase transition occurs at convenient temperatures in the bulk (although T_C is dependent on x), and the spontaneous polarizations and strains of $Pb(Zr_xTi_{1-x})O_3$ are large.

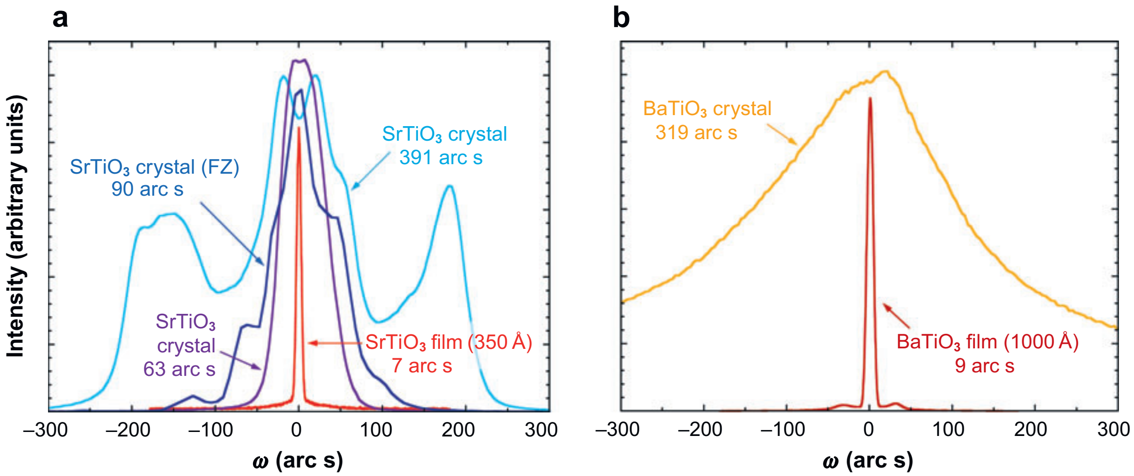

Figure 14

(*a*) Rocking curves and full width at half maximum (FWHM) of three commercial $SrTiO_3$ single crystals [one grown by floating zone (FZ) and two grown by flame fusion] showing the variation in structural quality together with an epitaxial 350-Å-thick $SrTiO_3/DyScO_3$ film grown by MBE at 650°C under biaxial tension of $\varepsilon_s = +1.1\%$. Adapted from Reference 102. (*b*) Rocking curves and FWHM of a commercial $BaTiO_3$ single crystal and an epitaxial 1000-Å-thick $BaTiO_3/GdScO_3$ film grown by MBE at 650°C under biaxial compression of $\varepsilon_s = -1.0\%$.

Strained $(001)_p$ $BaTiO_3$ Films

The ferroelectric properties of $BaTiO_3$ thin films have been dramatically enhanced through the use of biaxial compressive strains up to 1.7% imposed by coherent epitaxial film growth on $\mathit{Re}ScO_3$ substrates (21). In addition to a significant increase in the remanent polarization (P_r), T_C was increased by nearly 500°C (21). To establish T_C, a combination of techniques was employed because of the high temperatures involved and the electrical leakage of the thin $BaTiO_3$ films at high temperatures. The conventional test for ferroelectricity, hysteresis measurements, was used at room temperature to establish ferroelectricity. Then, SHG and the temperature dependence of the out-of-plane lattice parameter were measured from the temperature of the hysteresis loops to where kinks were seen in the temperature-dependent XRD (**Figure 13**) and SHG (**Figure 10**) to establish T_C. The temperatures seen by both methods were in agreement with each other and with the predictions of thermodynamic analysis (21).

Remanent polarization (P_r): the macroscopic polarization that remains at the surface of a ferroelectric with zero applied electric field

The resulting ferroelectric properties are comparable to those exhibited by unstrained $Pb(Zr_xTi_{1-x})O_3$, but in a more environmentally benign composition that is free of lead. These results demonstrate how strain can be used as a route to a lead-free ferroelectric for device applications, e.g., nonvolatile memories and electro-optic devices.

FERROELECTRIC SUPERLATTICES: THEORY AND EXPERIMENTS

Epitaxy: the growth of a film on a substrate whereby the arrangement of the atoms in the film is inherited from the arrangement of the atoms in the underlying substrate

MBE: molecular-beam epitaxy

MOCVD: metalorganic chemical vapor deposition

Thin film techniques offer powerful ways to assemble new materials, including metastable ones, that cannot be made by other methods. For single-layer films, metastable materials may be accessed through epitaxial stabilization (106–108). Here appropriate substrates are chosen to provide an interfacial free energy bias that for sufficiently thin films can overcome the volume free energy differences between polymorphs to make a desired metastable form have the lower total free energy (volume + interfacial free energies). In multilayer films the tremendous difference between the diffusion coefficient at the surface of the growing thin film compared with the much lower diffusion coefficient within the bulk of the film, including buried interfaces, makes it possible to make two-phase mixtures of end-member phases, in which in bulk solid solutions would exist. This is employed in the synthesis of many compound semiconductor device structures (7), e.g., AlAs/GaAs heterostructures, which are metastable heterostructures because their solid solution has a lower free energy over their entire composition range (109, pp. 126, 130). Similarly, heterostructures involving ferroelectrics such as $PbTiO_3/SrTiO_3$ or $BaTiO_3/SrTiO_3$ are metastable; it is energetically favorable for these oxides to dissolve into each other, forming $(Pb,Sr)TiO_3$ and $(Ba,Sr)TiO_3$ solid solutions (110; 111, p. 195). As **Figure 15** shows, the interface abruptness and layer thickness control of today's oxide superlattices involving ferroelectrics (34, 68–74) are comparable to what has become commonplace for AlAs/GaAs superlattices grown by molecular-beam epitaxy (MBE) (112) and metalorganic chemical vapor deposition (MOCVD) (113).

Superlattices consisting of a periodic stacking of thin ferroelectric and nonferroelectric perovskite layers have been predicted (75, 114–117) or reported (25, 30, 71, 72, 118–121) to possess many improved physical properties over homogeneous thin films of the same compositions. Among the improved properties are reported enhancements of dielectric constants and P_r in short-period two-component (118, 120, 121) and three-component (72) superlattices. Such reports need to be

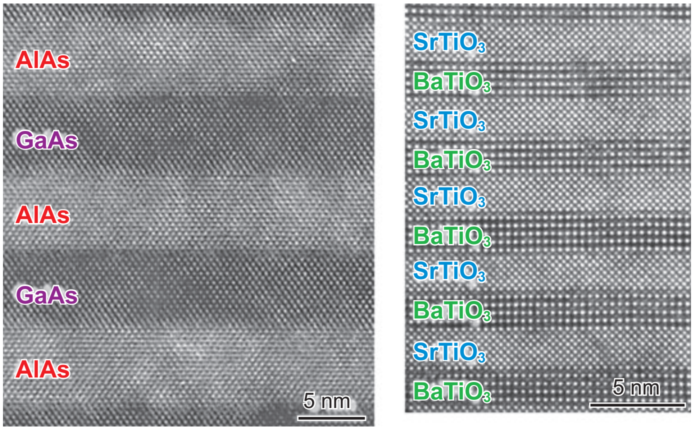

Figure 15

High-resolution transmission electron microscopy (TEM) images of GaAs/AlAs (reprinted from Reference 112, with permission; copyright 2002, Wiley-VCH; *left*) and $BaTiO_3/SrTiO_3$ (reprinted from Reference 70, with permission; copyright 2001, Elsevier; *right*) superlattices grown by molecular-beam epitaxy (MBE).

carefully evaluated because the movement of space charge in the superlattices can spuriously produce an apparent significant enhancement of dielectric constant (122, 123). The improved properties, however, could result from the large lattice mismatch, leading to huge strains for commensurate epitaxial growth (72, 118, 120, 121).

Layered heterostructures including superlattices are just one type of epitaxial composite involving ferroelectrics. Epitaxial heterostructures that make use of phase separation to form connectivities beyond the 2-2 connectivity (124) of superlattices are also being explored by thin film techniques. These include 1-3 epitaxial nanocomposites involving pillars of magnetic oxides in a ferroelectric matrix (125) or pillars of ferroelectric oxides in a magnetic matrix (126). Such heterostructures are being explored in ferroelectric systems to enhance the coupling between ferroelectric and magnetic oxides and thus form artificial magneto-electric heterostructures.

Artificially layered ferroelectric superlattices have enormous appeal from both a technological and a fundamental standpoint. The degree of control that can be achieved with modern deposition techniques is astounding, and superlattices with essentially perfect interfaces and single-unit-cell constituent layers are well within our grasp. In terms of technology, ferroelectric superlattices with appropriate electrical and mechanical boundary conditions hold the potential of tailoring ferroelectric properties precisely for an application. There are some indications that under certain circumstances the properties of a superlattice of two or more materials may be far superior to the parent materials from which they have been fabricated.

Crucial to the enlightened (non-Edisonian) synthesis of superior materials is an understanding of how the properties of the resulting superlattice material are related to those of the parent materials used. In superlattices in which the in-plane lattice parameter of all the constituents is constrained to that of the underlying substrate, the primary interaction that determines the overall properties of the superlattice seems to be electrostatic; the principal consideration is the minimization of polarization mismatch between layers, any mismatch giving rise to very high electrostatic energy penalties (116). This does not restrict the possibility of strain engineering, as the elastic constraint imposed by the substrate is an important factor in determining the orientation of the polarization in the superlattice layers and thus has a dramatic effect on the properties of the superlattice. Similarly, should a superlattice suffer relaxation owing to misfit dislocations, changes in the orientation of the polarization can arise, as seen in the $SrTiO_3$ layers of relaxed $BaTiO_3/SrTiO_3$ superlattices (127, 128). Beyond the commercial appeal of precisely tailored exceptional materials, these systems also allow an extraordinary opportunity for the exploration of the fundamentals of ferroelectricity. In essence, one can produce a system whose physics is defined by ultrathin components and interfaces, but with a larger total sample size allowing simple, precise characterization and a detailed exploration of the physics of ferroelectricity in strained ultrathin systems.

$(001)_p$ $PbTiO_3/(001)_p$ $SrTiO_3$ Superlattices

$PbTiO_3/SrTiO_3$ is an attractive combination: At room temperature the in-plane lattice parameter of (001) $PbTiO_3$ is an excellent match to the cubic lattice parameter of (001) $SrTiO_3$, allowing straightforward coherent growth of a (001) $PbTiO_3/(001)_p$ $SrTiO_3$ superlattice on a conducting Nb-doped (100) $SrTiO_3$ substrate. Owing to the similarities between the materials in the superlattice we can expect all interactions besides electrostatics to be minimized. To test this idea, Dawber et al. (73) fabricated a number of such $PbTiO_3/SrTiO_3$ superlattices, using off-axis radio frequency magnetron sputtering in which the $PbTiO_3$ layer thickness was varied while the $SrTiO_3$ layer thickness was maintained at three unit cells. The average *c*-axis lattice parameter was measured via XRD and used as a probe of the ferroelectric polarization. In thin films, as the film thickness is decreased, imprecision is introduced as the diffraction peak is broadened, owing to the finite thickness of the film. Bearing this and the reduction in signal strength in mind, determination of the tetragonality of the film is possible but takes a great deal of time and care. In contrast, for superlattices, although it is difficult to extract the individual lattice parameters of the constituent layers, the average lattice parameter is easily and accurately extracted from XRD measurements. When the $PbTiO_3$ layer is thicker than the $SrTiO_3$ layer, electrostatics can describe the behavior of the system well; electrostatics forces the polarization in both layers to be similar and decreases the magnitude of the polarization as the $PbTiO_3$ volume fraction is reduced (73). For samples in which the $PbTiO_3$ layer is thinner than the $SrTiO_3$ layer, however, the polarization is seen to recover strongly. PFM measurements have confirmed this result (73). The ability to use PFM is another appeal of studying the effect of strain on very thin ferroelectric layers in superlattices; thin films of only a few-unit-cell total thickness are too thin to be electrically written and probed by PFM, but there is no such problem for a superlattice, whose total thickness can be chosen to suit the measurement while extremely thin constituent layers are maintained.

Through the use of an electrostatic model, it was found that, as in constrained $(001)_p$ $BaTiO_3/(001)_p$ $SrTiO_3$ superlattices (116, 128), much of the behavior in constrained $(001)_p$ $PbTiO_3/(001)_p$ $SrTiO_3$ superlattices (73) could be understood via the concept that the two materials are forced to have similar polarizations because of the electrostatic energy cost involved in having different polarizations in the adjacent layers. The magnitude of the polarization is then determined by the balance between the energy cost or benefit of polarization of the two materials. The anomalous recovery cannot be understood on this basis and furthermore did not appear in full first-principles simulations of $(001)_p$ $PbTiO_3/(001)_p$ $SrTiO_3$ superlattices. This suggests that closer attention needs to be paid to aspects that do not appear naturally in these theoretical approaches, such as the exact nature of the interfaces in the system (both those between superlattice layers and also the substrate-superlattice interface), conduction processes, the possibility of the formation of new entropically stabilized phases similar to that predicted to occur under negative hydrostatic pressure by Tinte et al. (129), or the formation of multiple domains (130).

$(001)_p$ $BaTiO_3/(001)_p$ $SrTiO_3$ Superlattices

$(001)_p$ $BaTiO_3/(001)_p$ $SrTiO_3$ superlattices have also been extensively studied to investigate the effect of strain on thin layers of the ferroelectric $BaTiO_3$. In a recent study (74), these superlattices were grown on (100) $SrTiO_3$ substrates, and the $(001)_p$

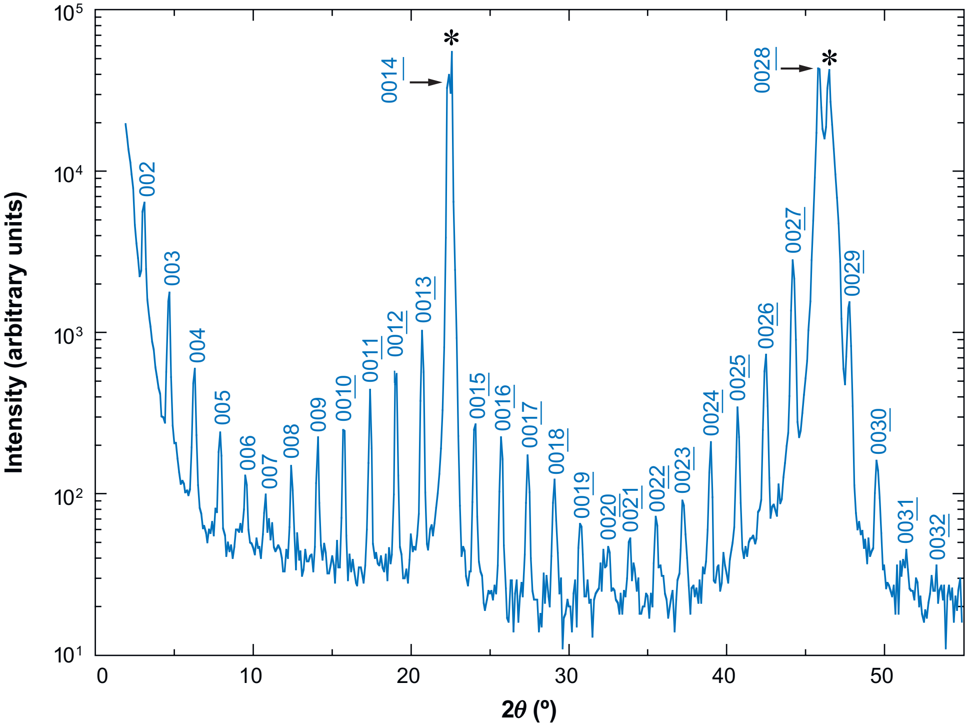

Figure 16

θ-2θ X-ray diffraction scan of a $[(BaTiO_3)_1/(SrTiO_3)_{13}]_{20}$ superlattice grown on (100) $SrTiO_3$. The substrate peaks are marked by asterisks (*), and the superlattice peaks are indexed according to the out-of-plane repeat wavelength $(BaTiO_3)_1/(SrTiO_3)_{13}$ ($n = 1$ and $m = 13$), which was repeated 20 times to form the superlattice.

$BaTiO_3$ layer in the superlattice was varied from 1 to 8 unit cells in thickness, whereas the $(001)_p$ $SrTiO_3$ spacer layer thickness was fixed to be either 4 unit cells or 13 unit cells thick. These superlattices can be denoted by $(BaTiO_3)_n/(SrTiO_3)_m$, where n and m refer to the thickness, in unit cells, of the $(001)_p$ $BaTiO_3$ and $(001)_p$ $SrTiO_3$ layers, respectively. The regularity of these superlattices grown by MBE is demonstrated by the presence and sharpness of all of the superlattice reflections in their XRD patterns. **Figure 16** shows an example of the $(BaTiO_3)_1/(SrTiO_3)_{13}$ superlattice studied, with $n = 1$ and $m = 13$.

Characterizing the resulting superlattices by UV Raman (*a*) made it possible to confirm the prediction that the unstrained $SrTiO_3$ layer in these superlattices is polarized owing to the electrostatic effect described above and (*b*) enabled the T_C of the ferroelectric superlattice to be established. **Figure 17** shows T_C as a function of n for a series of superlattices with $m = 4$ and $m = 13$, together with two different phase-field models of these superlattices. When the phase-field model is limited to a single-domain assumption (dashed lines in **Figure 17**), the agreement between theory and experiment is good for $m = 4$ but poor for $m = 13$. Put another way,

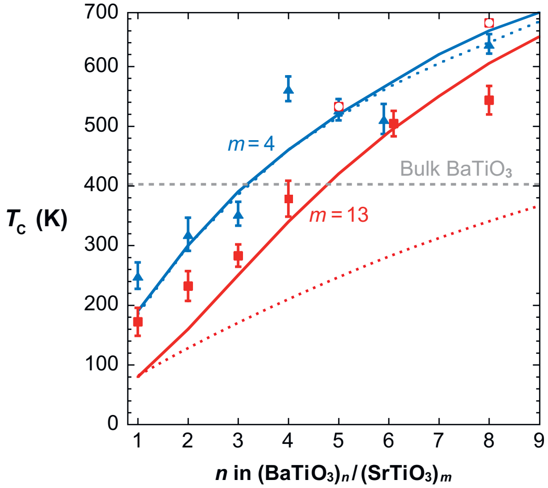

Figure 17

The dependence of T_C on n and m in $(BaTiO_3)_n/(SrTiO_3)_m$ superlattices. The blue symbols are for $m = 4$, and red symbols are for $m = 13$. T_C was determined by UV Raman (*closed symbols*) and temperature-dependent X-ray diffraction (XRD) (*open symbols*) measurements. A phase-field model with a single domain assumption yields the dashed curves. The solid lines are from full three-dimensional phase-field calculations. The T_C of bulk unstrained $BaTiO_3$ is also shown (adapted from Reference 74).

the $(001)_p$ $BaTiO_3/(001)_p$ $SrTiO_3$ superlattices show disagreement with theory when the $BaTiO_3$ layer is thinner than the $SrTiO_3$ layer, just as was seen for the $(001)_p$ $PbTiO_3/(001)_p$ $SrTiO_3$ superlattices described above. First-principles calculations also operate under a single-domain assumption because of the limited number of atoms in the calculation. When a full three-dimensional phase-field simulation is performed (solid lines in **Figure 17**), the agreement between theory and experiment becomes good for both $m = 4$ and $m = 13$ over the entire range. These calculations indicate that the low-energy configuration is a multiple-domain state, which allows the polarization in the $(001)_p$ $SrTiO_3$ layers to drop considerably when the $(001)_p$ $BaTiO_3$ layer is much thinner than the $(001)_p$ $SrTiO_3$ layer and results in a significant increase of T_C compared with the single-domain state (74).

With full first-principles methods, it is currently possible to investigate superlattices of up to approximately period 10, yielding full microscopic information about the atomic and electronic structure, polarization, zone-center phonons, and dielectric response. Systems for which results have been reported include $BaTiO_3/SrTiO_3$ (116, 128), $PbTiO_3/SrTiO_3$ (73), and an assortment of two-component and three-component systems containing $CaTiO_3$, $SrTiO_3$, and $BaTiO_3$, with varying epitaxial strain (75). Some interesting features emerge. For example, superlattices of even a single-unit-cell-thick layer of $BaTiO_3$ and $PbTiO_3$ with $SrTiO_3$ have a ferroelectric ground state. These predictions have been verified experimentally (73, 74). With a 1 × 1 lateral supercell and *P4mmm* symmetry, $CaTiO_3$ has a polarization even larger than that of $BaTiO_3$, resulting from the suppression of the oxygen octahedral rotational and tilting instabilities (75). This latter feature is strongly dependent on a sufficient thickness of the $CaTiO_3$ layer, with a single layer showing no significant polarization.

On the basis of these results, a class of simple models has been developed. The starting point is to treat the component layers as bulk materials under the appropriate mechanical and electrical boundary conditions (73, 116). The effects of in-plane epitaxial strain are obtained from first-principles calculations for bulk material with constrained lattice vectors (131). The full first-principles results so far obtained for $PbTiO_3$ (132), $SrTiO_3$ (133), $BaTiO_3$ (78), and $BiFeO_3$ (134) have been extended to an additional five perovskite oxides through the use of a parameterized form for the total energy (135). The in-plane strain leads to changes in the unconstrained lattice vectors; for example, compressive in-plane strain increases the tetragonality of *P*4*mm* $BaTiO_3$. A characteristic property of perovskites, although not of all ferroelectric oxides (136), is that the change in strain state is strongly coupled to changes in the polarization. For example, for compressed $BaTiO_3$ an increase in tetragonality produces a substantial increase in the in-plane polarization. In the superlattice, the local polarization of each unit-cell layer is defined through the use of the atomic displacements from a centrosymmetric reference structure and Born effective charges. Considerations of electrostatic energy dominate, favoring superlattices with zero macroscopic electric field and a constant normal component of the polarization; the energy cost of nonzero fields can be obtained by first-principles computations of bulk materials (137, 138) in nonzero electric fields. The most stable superlattice structures thus are those that have low in-plane lattice mismatch and good polarization matching. Strain-enhanced polarization can be readily achieved; $BaTiO_3/SrTiO_3$ superlattices on $SrTiO_3$ substrates show polarizations above bulk $BaTiO_3$ for $BaTiO_3$ content of greater than 50% (116). A phase-field approach by solving the coupled micromechanics, electrostatics, and equilibrium equation for the polarization distribution predicts the transition temperatures and polarization distributions for a number of $BaTiO_3/SrTiO_3$ superlattices, which are in excellent agreement with the measured values from UV Raman spectroscopy (74). Superlattice strain and fields can also stabilize nonbulk phases, such as ferroelectric $SrTiO_3$ (20, 133). Thicker layers have been studied using interatomic potentials (77).

As the database of first-principles results grows, refinements to this basic model are suggested. In particular, the above example of constraining the symmetry of $CaTiO_3$ suggests a generalization to a model of interacting unit-cell layers (117). For three-component superlattices, additional terms sensitive to the relative orientation of the polarization and the interface can be added to reproduce the up-down asymmetry in the polarization associated with the inversion symmetry breaking (115). Depending on the materials combinations, the interfaces may involve nonbulk atomic and electronic rearrangement and require additional modeling. Energy associated with atomic-scale bonding arrangements in the interface may in some configurations be sufficient to dominate over the electrostatic and strain energies, especially with ultrathin layers in which the interface density is high. Identification and investigation of relevant materials combinations would guide the development of interface terms in such cases.

APPLICATION OPPORTUNITIES

FeRAM: ferroelectric random-access memory

Although the focus of this review has been on scientific challenges, many important applications are moving toward the utilization of ferroelectric constituents that are truly nanoscale. Examples include tunable dielectrics for which degradation in interface behavior severely impacts performance, high-density nonvolatile memories that can be scaled for deep submicron cell sizes, and ferroelectric storage media for scanning probe–based memories (34, 103).

The significant enhancements in T_C and P_r in strained ferroelectrics can be used in applications suited for thin ferroelectric films (for which large strains to enhance T_C and P_r can be achieved without film cracking). Ferroelectric random-access memory (FeRAM) are one such application for the introduction of more environmentally benign ferroelectrics that attain the properties of current bulk ferroelectric materials via strain. The major disadvantages of the two materials most widely being pursued for FeRAM (139), $Pb(Zr,Ti)O_3$ and $SrBi_2Ta_2O_9$, are (*a*) the volatility of the lead and bismuth constituents of these materials, which complicates their introduction into semiconductor fabrication facilities, and (*b*) environmental issues associated with the toxicity of lead. The potential of strain to enhance a lead-free ferroelectric composition is just beginning to be explored, but the ferroelectric properties of strained $BaTiO_3$ are already suitable for ferroelectric memory applications (21), provided these properties can be achieved on technologically important substrates, e.g., silicon.

Although the structural quality of perovskite films grown on semiconductor substrates is far from the quality of perovskites grown on perovskite substrates, significant improvements have been made over the past two decades since perovskites were first epitaxially integrated with semiconductors (140). There are now several routes for the epitaxial integration of perovskites with semiconductors including (100) Si (140–142), (100) Ge (142), (100) GaAs (143, 144), and (0001) GaN (145, 146). Via these means, a multitude of ferroelectrics, with conducting top and bottom electrodes when desired, have been epitaxially integrated with semiconductor materials (140, 142, 145, 146). This capability may play a significant role in future hybrid devices.

The emerging experimental and theoretical capabilities in short-period superlattices open up promising avenues to design and create new artificially structured materials with unprecedented properties. With modeling of first-principles results, it is possible to search a large parameter space of materials and layer-thickness sequences to identify nontrivial candidates to produce, optimize, or tune desired properties. Extending the exploration of the strain-electric-field phase diagrams to more materials will lead to the identification of nonbulk phases by appropriate boundary conditions, for example, highly polar states of bulk paraelectrics, ferroelectric states for bulk antiferroelectric or antiferrodistortive compounds, and low-symmetry monoclinic or triclinic polar states with large dielectric and piezoelectric responses. Even more novel behavior can be obtained by pursuing the investigation of distinctive interfaces, with order parameters distinct from the surrounding matrix, and by building up superlattice materials in which interface properties dominate. Layer sequences that lack inversion symmetry in superlattices give freedom in tailoring gradients of the polarization that can be tuned by the choice of sequence details. The inclusion of solid solutions as superlattice components will become feasible, with the possibility of accessing nonbulk compositions through the use of epitaxial stabilization (106–108). Novel magnetic behavior can also be expected; magnetic ordering could be stabilized in bulk nonmagnetic materials under the electrical and mechanical boundary conditions of the superlattice. There is also increasing interest in the incorporation of magnetic materials into the superlattice. First-principles studies of magnetic ferroelectric oxides, such as hexagonal manganites (147, 148), have been demonstrated to be accurate and are ripe for extension to predicting the behavior of superlattices. These strategies may provide a path to enhance magnetic ferroelectrics with entirely new coupling mechanisms between the magnetic and ferroelectric order parameters, allowing switching to occur by spin-phonon interactions rather than elastic interactions (149).

Strong coupling between the magnetic and ferroelectric order parameters via a spin-phonon interaction was recently predicted to occur in appropriately strained $EuTiO_3$ (150). Although unstrained $EuTiO_3$ is paraelectric and antiferromagnetic at low temperatures, first-principle calculations indicate that $(001)_p$ $EuTiO_3$ under a biaxial compressive strain of $\sim 1\%$ $EuTiO_3$ is on the verge of a transition to a ferroelectric and ferromagnetic state. For such strained $EuTiO_3$ films, the application of a modest electric field of order 10^5 V cm^{-1} is predicted to induce ferromagnetism with a magnetization of 7 μ_B per europium atom. Similarly, the application of a modest magnetic field of order 1 T is predicted to induce ferroelectricity with a spontaneous polarization of ~ 10 μC cm^{-2} (150). The predicted coupling between the magnetic and ferroelectric order parameters in this strain-enabled material is orders of magnitude larger than any known multiferroic and a fantastic opportunity for strain tuning.

SUMMARY POINTS

1. Percent-level strains can have a tremendous effect on the properties of ferroelectric thin films and superlattices. They can make materials that are not ferroelectric at any temperature ferroelectric. They can enhance T_C by hundreds of degrees and simultaneously enhance P_r.
2. Although bulk ferroelectric oxides normally break long before they are strained to percent levels, such strains are readily applied to ferroelectric thin films through the use of epitaxy on appropriate substrates.
3. The maturity, power, and complementary nature of theoretical approaches, including first principles, thermodynamic analysis, and phase-field models, to accurately predict the properties of strained ferroelectrics bode well for the future of theory-driven research in this area. The huge changes in properties resulting from strain, first quantitatively predicted by theory, have been borne out in experiment. Also in agreement with theory is the observation of ferroelectricity in superlattices containing layers of bulk ferroelectric materials just one unit cell in thickness, provided that appropriate mechanical and electrical boundary conditions are met.

4. A broad range of suitable substrates that are appropriate for ferroelectric thin film and superlattice growth have been developed, with good progress toward large-size, commercially viable solutions. Advances in ferroelectric film deposition have led to materials with excellent structural and electrical properties.

FUTURE ISSUES

1. Improved theory is needed to (*a*) provide an understanding of the effects of strain and defects on coercive field and switching dynamics and (*b*) allow the huge parameter space of composition, strain, layer thickness, and gradients that are possible on an atomic-layer level in modern multilayer heterostructures to be intelligently navigated to enable a new era of theory-driven research yielding improved materials for society.
2. Improved substrates and film synthesis techniques are necessary to customize the strain and composition in ferroelectric films and superlattices with greater precision and allow a multitude of new directions to be explored: all-interface systems, new epitaxially stabilized artificial materials, and exotic polarization states, e.g., by clamping $CaTiO_3$ and preventing its octahedra from rotating.
3. Improved characterization tools—nanofocused and time-resolved XRD, time-resolved electron microscopy, and ultrafast SPM—are crucial to locally study switching dynamics in strained ferroelectrics.
4. Improved devices exploiting these advances are key to transition these benefits to society. Such devices include strained ferroelectrics with enhanced nonlinear optical coefficients for modulators; strain-enhanced ferroelectrics that offer breakthrough electromechanical performance for nanoscale actuation and sensing; strain-enhanced ferroelectrics that are simultaneously ferromagnetic for dual electric- and magnetic-field-tunable microwave and optical devices; strain-enhanced antiferroelectrics for improved energy storage; and more environmentally benign strain-enhanced ferroelectric compositions that can replace lead-containing ferroelectric in applications for improved health and safety.

ACKNOWLEDGMENTS

We gratefully acknowledge our colleagues and collaborators for sharing their insights and helping us to explore and better understand the exciting area of strained ferroelectric thin films. We especially thank P. Aebi, A. Antons, O. Auciello, G.R. Bai, M.D. Biegalski, D.H.A. Blank, E. Bousquet, C.D. Brandle, A. Bruchhausen, C. Bungaro, A. Cantarero, M. Cantoni, W. Chang, Y.B. Chen, K.J. Choi, S. Choudhury, H.-M. Christen, F. Clerc, B. Craigo, L.E. Cross, M. Dawber, L. Despont, O. Diéguez, J.A. Eastman, A. Fainstein, C.J. Fennie, D.D. Fong, V.J. Fratello, P.H. Fuoss, F.J. Garcia de Abajo, M.G. Garnier, P. Ghosez, V. Gopalan, J.H. Haeni, M.E. Hawley, T. Heeg, X.Y. Huang, P. Irvin, Q.X. Jia, J. C. Jiang, K. Johnston, J. Junquera, R.S. Katiyar, D.M. Kim, S.W. Kirchoefer, H. Kohlstedt, C. Koitzsch, A. Kumar, N.D. Lanzillotti-Kimura, J. Lettieri, J. Levy, Y.L. Li, C. Lichtensteiger, F. Lichtenberg, H.Z. Ma, J. Mannhart, A. Munkholm, M.V.R. Murty, V. Nagarajan, S.M. Nakhmanson, J.B. Neaton, R.E. Newnham, X.Q. Pan, R. Ramesh, P. Reiche, J. Rodriguez-Contreras, J. Schubert, A. Sharan, V. Sherman, A. Soukiassian, N.A. Spaldin, G.B. Stephenson, H.P. Sun, A.K. Tagantsev, D.A. Tenne, C.D. Theis, C. Thompson, L. Tian, W. Tian, S. Tinte, S. Trolier-McKinstry, R. Uecker, V. Vaithyanathan, D. Vanderbilt, A. Vasudevarao, M. Veithen, A.J. Ven Graitis, X.X. Xi, and M. A. Zurbuchen. We gratefully acknowledge the financial support of the National Science Foundation under Grant Nos. DMR-0507146, DMR-0122638, DMR-0213623, DMR-0313764, and ECS-0210449; the Office of Naval Research under Grant Nos. N00014-03-1-0721, N00014-04-1-0426, and N00014-05-1-0559, monitored by Dr. Colin Wood, and N00014-00-1-0261 and N00014-01-1-0365. The work at Argonne is supported by the U.S. Department of Energy under Contract No. DE-AC02-06CH11357. Part of this work was supported by the Swiss National Science Foundation through the National Center of Competence in Research "Materials with Novel Electronic Properties-MaNEP" and Division II, and ESF (Thiox).

LITERATURE CITED

1. Merz WJ. 1950. The effect of hydrostatic pressure on the Curie point of barium titanate single crystals. *Phys. Rev.* 77:52–54
2. Samara GA. 1966. Pressure and temperature dependences of the dielectric properties of the perovskites $BaTiO_3$ and $SrTiO_3$. *Phys. Rev.* 151:378–86
3. Goswami AK, Cross LE. 1968. Pressure and temperature dependence of the dielectric properties of the perovskite barium titanate. *Phys. Rev.* 171:549–50
4. Griffith AA. 1920. The phenomena of rupture and flow in solids. *Philos. Trans. R. Soc. London Ser. A* 221:163–98
5. Klokholm E, Matthews JW, Mayadas AF, Angilello J. 1972. Epitaxial strains and fracture in garnet films. In *Magnetism and Magnetic Materials*, ed. CD Graham, JJ Rhyne, pp. 105–9. New York: Am. Inst. Phys.
6. Freund LB, Suresh S. 2003. *Thin Film Materials: Stress, Defect Formation and Surface Evolution*. Cambridge, UK: Cambridge Univ. Press. 768 pp.
7. Nguyen LD, Brown AS, Thompson MA, Jelloian LM. 1992. 50-nm self-aligned-gate pseudomorphic AlInAs/GaInAs high electron mobility transistors. *IEEE Trans. Electron. Devices* 39:2007–14
8. Welser J, Hoyt JL, Gibbons JF. 1994. Electron mobility enhancement in strained-Si *n*-type metal-oxide-semiconductor field-effect transistors. *IEEE Electron. Device Lett.* 15:100–2
9. Beach RS, Borchers JA, Matheny A, Erwin RW, Salamon MB, et al. 1993. Enhanced Curie temperatures and magnetoelastic domains in Dy/Lu superlattices and films. *Phys. Rev. Lett.* 70:3502–5

10. Gan Q, Rao RA, Eom CB, Garrett JL, Lee M. 1998. Direct measurement of strain effects on magnetic and electrical properties of epitaxial $SrRuO_3$ thin films. *Appl. Phys. Lett.* 72:978–80
11. Lock JM. 1951. Penetration of magnetic fields into superconductors. III. Measurements on thin films of tin, lead and indium. *Proc. R. Soc. London* A208:391–408
12. Sato H, Naito M. 1997. Increase in the superconducting transition temperature by anisotropic strain effect in (001) $La_{1.85}Sr_{0.15}CuO_4$ thin films on $LaSrAlO_4$ substrates. *Phys. C* 274:221–26
13. Bozovic I, Logvenov G, Belca I, Narimbetov B, Sveklo I. 2002. Epitaxial strain and superconductivity in $La_{2-x}Sr_xCuO_4$ thin films. *Phys. Rev. Lett.* 89:107001
14. Devonshire AF. 1954. Theory of ferroelectrics. *Philos. Mag.* 3(Suppl.):85–130
15. Pertsev NA, Zembilgotov AG, Tagantsev AK. 1998. Effect of mechanical boundary conditions on phase diagrams of epitaxial ferroelectric thin films. *Phys. Rev. Lett.* 80:1988–91
16. Pertsev NA, Koukhar VG. 2000. Polarization instability in polydomain ferroelectric epitaxial thin films and the formation of heterophase structures. *Phys. Rev. Lett.* 84:3722–25
17. Pertsev NA, Tagantsev AK, Setter N. 2000. Phase transitions and strain-induced ferroelectricity in $SrTiO_3$ epitaxial thin films. *Phys. Rev. B* 61:R825–29. Erratum. 2002. *Phys. Rev. B* 65:219901
18. Koukhar VG, Pertsev NA, Waser R. 2001. Thermodynamic theory of epitaxial ferroelectric thin films with dense domain structures. *Phys. Rev. B* 64:214103
19. Li YL, Hu SY, Liu ZK, Chen LQ. 2001. Phase-field model of domain structures in ferroelectric thin films. *Appl. Phys. Lett.* 78:3878–80
20. Haeni JH, Irvin P, Chang W, Uecker R, Reiche P, et al. 2004. Room-temperature ferroelectricity in strained $SrTiO_3$. *Nature* 430:758–61
21. Choi KJ, Biegalski M, Li YL, Sharan A, Schubert J, et al. 2004. Enhancement of ferroelectricity in strained $BaTiO_3$ thin films. *Science* 306:1005–9
22. Li YL, Chen LQ. 2006. Temperature-strain phase diagram for $BaTiO_3$ thin films. *Appl. Phys. Lett.* 88:072905
23. Li YL, Choudhury S, Haeni JH, Biegalski MD, Vasudevarao A, et al. 2006. Phase transitions and domain structures in strained pseudocubic (100) $SrTiO_3$ thin films. *Phys. Rev. B* 73:184112
24. Specht ED, Christen HM, Norton DP, Boatner LA. 1998. X-ray diffraction measurement of the effect of layer thickness on the ferroelectric transition in epitaxial $KTaO_3/KNbO_3$ multilayers. *Phys. Rev. Lett.* 80:4317–20
25. Christen HM, Knauss LA, Harshavardhan KS. 1998. Field-dependent dielectric permittivity of paraelectric superlattice structures. *Mater. Sci. Eng. B* 56:200–3
26. Christen HM, Specht ED, Norton DP, Chisholm MF, Boatner LA. 1998. Long-range ferroelectric interactions in $KTaO_3/KNbO_3$ superlattice structures. *Appl. Phys. Lett.* 72:2535–37
27. Abe K, Yanase N, Sano K, Izuha M, Fukushima N, Kawakubo T. 1998. Modification of ferroelectricity in heteroepitaxial (Ba,Sr)TiO_3 films for non-volatile memory applications. *Integr. Ferroelectr.* 21:197–206

28. Yanase N, Abe K, Fukushima N, Kawakubo T. 1999. Thickness dependence of ferroelectricity in heteroepitaxial $BaTiO_3$ thin film capacitors. *Jpn. J. Appl. Phys.* 38(Pt. 1):5305–8
29. Streiffer SK, Eastman JA, Fong DD, Thompson C, Munkholm A, et al. 2002. Observation of nanoscale 180° stripe domains in ferroelectric $PbTiO_3$ thin films. *Phys. Rev. Lett.* 89:067601
30. Christen HM, Specht ED, Silliman SS, Harshavardhan KS. 2003. Ferroelectric and antiferroelectric coupling in superlattices of paraelectric perovskites at room temperature. *Phys. Rev. B* 68:20101
31. Wurfel P, Batra IP, Jacobs JT. 1973. Polarization instability in thin ferroelectric films. *Phys. Rev. Lett.* 30:1218–21
32. Batra IP, Wurfel P, Silverman BD. 1973. Phase transition, stability and depolarization field in ferroelectric thin films. *Phys. Rev. B* 8:3257–65
33. Junquera J, Ghosez P. 2003. Critical thickness for ferroelectricity in perovskite ultrathin films. *Nature* 422:506–9
34. Ahn CH, Rabe KM, Triscone JM. 2004. Ferroelectricity at the nanoscale: local polarization in oxide thin films and heterostructures. *Science* 303:488–91
35. Fong DD, Stephenson GB, Streiffer SK, Eastman JA, Auciello O, et al. 2004. Ferroelectricity in ultrathin perovskite films. *Science* 304:1650–53
36. Fong DD, Kolpak AM, Eastman JA, Streiffer SK, Fuoss PH, et al. 2006. Stabilization of monodomain polarization in ultrathin $PbTiO_3$ films. *Phys. Rev. Lett.* 96:27601
37. Speck JS, Daykin AC, Seifert A, Romanov AE, Pompe W. 1995. Domain configurations due to multiple misfit relaxation mechanisms in epitaxial ferroelectric thin films. III. Interfacial defects and domain misorientations. *J. Appl. Phys.* 78:1696–706
38. Nix WD, Clemens BM. 1999. Crystallite coalescence: a mechanism for intrinsic tensile stresses in thin films. *J. Mater. Res.* 14:3467–73
39. Taylor TR, Hansen PJ, Acikel B, Pervez N, York RA, et al. 2002. Impact of thermal strain on the dielectric constant of sputtered barium strontium titanate thin films. *Appl. Phys. Lett.* 80:1978–80
40. Canedy CL, Li H, Alpay SP, Salamanca-Riba L, Roytburd AL, Ramesh R. 2000. Dielectric properties in heteroepitaxial $Ba_{0.6}Sr_{0.4}TiO_3$ thin films: effect of internal stresses and dislocation-type defects. *Appl. Phys. Lett.* 77:1695–97
41. Misirlioglu IB, Vasiliev AL, Aindow M, Alpay SP, Ramesh R. 2004. Threading dislocation generation in epitaxial $(Ba,Sr)TiO_3$ films grown on (001) $LaAlO_3$ by pulsed laser deposition. *Appl. Phys. Lett.* 84:1742–44
42. Chu MW, Szafraniak I, Scholz R, Harnagea C, Hesse D, et al. 2004. Impact of misfit dislocations on the polarization instability of epitaxial nanostructured ferroelectric perovskites. *Nat. Mater.* 3:87–90
43. Alpay SP, Misirlioglu IB, Nagarajan V, Ramesh R. 2004. Can interface dislocations degrade ferroelectric properties? *Appl. Phys. Lett.* 85:2044–46
44. Nagarajan V, Jia CL, Kohlstedt H, Waser R, Misirlioglu IB, et al. 2005. Misfit dislocations in nanoscale ferroelectric heterostructures. *Appl. Phys. Lett.* 86:192910

45. Sandstrom RL, Giess EA, Gallagher WJ, Segmüller A, Cooper EI, et al. 1988. Lanthanum gallate substrates for epitaxial high-temperature superconducting thin films. *Appl. Phys. Lett.* 53:1874–76
46. Simon RW, Platt CE, Lee AE, Lee GS, Daly KP, et al. 1988. Low-loss substrate for epitaxial growth of high-temperature superconductor thin films. *Appl. Phys. Lett.* 53:2677–79
47. Koren G, Gupta A, Giess EA, Segmüller A, Laibowitz RB. 1989. Epitaxial films of $YBa_2Cu_3O_{7-\delta}$ on $NdGaO_3$, $LaGaO_3$, and $SrTiO_3$ substrates deposited by laser ablation. *Appl. Phys. Lett.* 54:1054–56
48. Feenstra R, Boatner LA, Budai JD, Christen DK, Galloway MD, Poker DB. 1989. Epitaxial superconducting thin films of $YBa_2Cu_3O_{7-x}$ on $KTaO_3$ single crystals. *Appl. Phys. Lett.* 54:1063–65
49. Giess EA, Sandstrom RL, Gallagher WJ, Gupta A, Shinde SL, et al. 1990. Lanthanide gallate perovskite-type substrates for epitaxial, high-T_c superconducting $Ba_2YCu_3O_{7-\delta}$ films. *IBM J. Res. Dev.* 34:916–26
50. Asano H, Kubo S, Michikami O, Satoh M, Konaka T. 1990. Epitaxial growth of $EuBa_2Cu_3O_{7-y}$ films on $YAlO_3$ single crystals. *Jpn. J. Appl. Phys.* 29(Pt. 2):L1452–54
51. Berkstresser GW, Valentino AJ, Brandle CD. 1991. Growth of single crystals of rare earth gallates. *J. Cryst. Growth* 109:457–66
52. Berkstresser GW, Valentino AJ, Brandle CD. 1991. Growth of single crystals of lanthanum aluminate. *J. Cryst. Growth* 109:467–71
53. Ralston RW, Kastner MA, Gallagher WJ, Batlogg B. 1992. Cooperating on superconductivity. *IEEE Spect.* 29(8):50–55
54. Berkstresser GW, Valentino AJ, Brandle CD. 1993. Congruent composition for growth of lanthanum aluminate. *J. Cryst. Growth* 128:684–88
55. Brown R, Pendrick V, Kalokitis D, Chai BHT. 1990. Low-loss substrate for microwave application of high-temperature superconductor films. *Appl. Phys. Lett.* 57:1351–53
56. Hontsu S, Ishii J, Kawai T, Kawai S. 1991. $LaSrGaO_4$ substrate gives oriented crystalline $YBa_2Cu_3O_{7-y}$ films. *Appl. Phys. Lett.* 59:2886–88
57. Mateika D, Kohler H, Laudan H, Volkel E. 1991. Mixed-perovskite substrates for high-T_c superconductors. *J. Cryst. Growth* 109:447–56
58. Phillips JM. 1996. Substrate selection for high-temperature superconducting thin films. *J. Appl. Phys.* 79:1829–48
59. Schubert J, Trithaveesak O, Petraru A, Jia CL, Uecker R, et al. 2003. Structural and optical properties of epitaxial $BaTiO_3$ thin films grown on $GdScO_3(110)$. *Appl. Phys. Lett.* 82:3460–62
60. Biegalski MD, Haeni JH, Trolier-McKinstry S, Schlom DG, Brandle CD, Ven Graitis AJ. 2005. Thermal expansion of the new perovskite substrates $DyScO_3$ and $GdScO_3$. *J. Mater. Res.* 20:952–58
61. Uecker R, Wilke H, Schlom DG, Velickov B, Reiche P, et al. 2006. Spiral formation during Czochralski growth of rare-earth scandates. *J. Cryst. Growth* 295:84–91
62. Kawasaki M, Takahashi K, Maeda T, Tsuchiya R, Shinohara M, et al. 1994. Atomic control of the $SrTiO_3$ crystal surface. *Science* 266:1540–42

63. Koster G, Kropman BL, Rijnders GJHM, Blank DHA, Rogalla H. 1998. Quasi-ideal strontium titanate crystal surfaces through formation of strontium hydroxide. *Appl. Phys. Lett.* 73:2920–22
64. Schrott AG, Misewich JA, Copel M, Abraham DW, Zhang Y. 2001. A-site surface termination in strontium titanate single crystals. *Appl. Phys. Lett.* 79:1786–88
65. Ohnishi T, Takahashi K, Nakamura M, Kawasaki M, Yoshimoto M, Koinuma H. 1999. A-site layer terminated perovskite substrate: $NdGaO_3$. *Appl. Phys. Lett.* 74:2531–33
66. Bae HJ, Sigman J, Norton DP, Boatner LA. 2005. Surface treatment for forming unit-cell steps on the (001) $KTaO_3$ substrate surface. *Appl. Surf. Sci.* 241:271–78
67. Dawber M, Rabe KM, Scott JF. 2005. Physics of thin-film ferroelectric oxides. *Rev. Mod. Phys.* 77:1083–130
68. Iijima K, Terashima T, Bando Y, Kamigaki K, Terauchi H. 1992. Atomic layer growth of oxide thin films with perovskite-type structure by reactive evaporation. *J. Appl. Phys.* 72:2840–45
69. Christen HM, Boatner LA, Budai JD, Chisholm MF, Géa LA, et al. 1996. The growth and properties of epitaxial $KNbO_3$ thin films and $KNbO_3/KTaO_3$ superlattices. *Appl. Phys. Lett.* 68:1488–90
70. Schlom DG, Haeni JH, Lettieri J, Theis CD, Tian W, et al. 2001. Oxide nano-engineering using MBE. *Mater. Sci. Eng. B* 87:282–91
71. Warusawithana MR, Colla EV, Eckstein JN, Weissman MB. 2003. Artificial dielectric superlattices with broken inversion symmetry. *Phys. Rev. Lett.* 90:036802
72. Lee HN, Christen HM, Chisholm MF, Rouleau CM, Lowndes DH. 2005. Strong polarization enhancement in asymmetric three-component ferroelectric superlattices. *Nature* 433:395–99
73. Dawber M, Lichtensteiger C, Cantoni M, Veithen M, Ghosez P, et al. 2005. Unusual behavior of the ferroelectric polarization in $PbTiO_3/SrTiO_3$ superlattices. *Phys. Rev. Lett.* 95:177601
74. Tenne DA, Bruchhausen A, Lanzillotti-Kimura ND, Fainstein A, Katiyar RS, et al. 2006. Probing nanoscale ferroelectricity by ultraviolet Raman spectroscopy. *Science* 313:1614–16
75. Nakhmanson SM, Rabe KM, Vanderbilt D. 2005. Polarization enhancement in two- and three-component ferroelectric superlattices. *Appl. Phys. Lett.* 87:102906
76. Sepliarsky M, Stachiotti MG, Migoni RL. 2005. Surface reconstruction and ferroelectricity in $PbTiO_3$ thin films. *Phys. Rev. B* 72:014110
77. Sepliarsky M, Phillpot SR, Stachiotti MG, Migoni RL. 2002. Ferroelectric phase transitions and dynamical behavior in $KNbO_3/KTaO_3$ superlattices by molecular-dynamics simulation. *J. Appl. Phys.* 91:3165–71
78. Diéguez O, Tinte S, Antons A, Bungaro C, Neaton JB, et al. 2004. Ab initio study of the phase diagram of epitaxial $BaTiO_3$. *Phys. Rev. B* 69:212101
79. Lai BK, Kornev IA, Bellaiche L, Salamo GJ. 2005. Phase diagrams of epitaxial $BaTiO_3$ ultrathin films from first principles. *Appl. Phys. Lett.* 86:132904
80. Íñiguez J, Ivantchev S, Perez-Mato JM, García A. 2001. Devonshire-Landau free energy of $BaTiO_3$ from first principles. *Phys. Rev. B* 63:144103

81. Li YL, Hu SY, Liu ZK, Chen LQ. 2002. Effect of substrate constraint on the stability and evolution of ferroelectric domain structures in thin films. *Acta Mater.* 50:395–411

81a. Pertsev NA, Kuhkar VG, Kohlstedt H, Waser R. 2003. Phase diagrams and physical properties of single-domain epitaxial $Pb(Zr_{1-x}\ Ti_x)O_3$ thin films. *Phys. Rev. B* 67:054107

81b. Li YL, Choudhury S, Liu ZK, Chen LQ. 2003. Effect of external mechanical constraints on the phase diagram of epitaxial $Pb(Zr_{1-x}\ Ti_x)O_3$ thin films: thermodynamic calculations and phase field simulations. *Appl. Phys. Lett.* 83:1608–10

82. Alexe M, Gruverman A, ed. 2004. *Nanoscale Characterisation of Ferroelectric Materials: Scanning Probe Microscopy Approach*. Berlin: Springer. 282 pp.

83. Stemmer S, Streiffer SK, Ernst F, Rühle M. 1995. Dislocations in $PbTiO_3$ films. *Phys. Status Solid. A* 147:135–54

84. Sun HP, Tian W, Pan XQ, Haeni JH, Schlom DG. 2004. Evolution of dislocation arrays in epitaxial $BaTiO_3$ thin films grown on (100) $SrTiO_3$. *Appl. Phys. Lett.* 84:3298–300

85. Misirlioglu IB, Vasiliev AL, Alpay SP, Aindow M, Ramesh R. 2006. Defect microstructures in epitaxial $PbZr_{0.2}Ti_{0.8}O_3$ films grown on (001) $SrTiO_3$ by pulsed laser deposition. *J. Mater. Sci.* 41:697–707

86. Sun HP, Pan XQ, Haeni JH, Schlom DG. 2004. Structural evolution of dislocation half-loops in epitaxial $BaTiO_3$ thin films during high-temperature annealing. *Appl. Phys. Lett.* 85:1967–69

87. Lichtensteiger C, Junquera J, Ghosez P, Triscone JM. 2005. Ferroelectricity and tetragonality in ultrathin $PbTiO_3$ films. *Phys. Rev. Lett.* 94:047603

88. Fuoss PH, Brennan S. 1990. Surface sensitive X-ray scattering. *Annu. Rev. Mater. Sci.* 20:365–90

89. Stephenson GB, Fong DD, Murty MVR, Streiffer SK, Eastman JA, et al. 2003. In situ X-ray studies of vapor phase epitaxy of $PbTiO_3$. *Phys. B* 336:81–89

90. Do DH, Evans PG, Isaacs ED, Kim DM, Eom CB, Dufresne EM. 2004. Structural visualization of polarization fatigue in epitaxial ferroelectric oxide devices. *Nat. Mater.* 3:365–69

91. Grigoriev A, Do DH, Kim DM, Eom CB, Adams B, et al. 2006. Nanosecond domain wall dynamics in ferroelectric $Pb(Zr,Ti)O_3$ thin films. *Phys. Rev. Lett.* 96:187601

92. Fong DD, Cionca C, Yacoby Y, Stephenson GB, Eastman JA, et al. 2005. Direct structural determination in ultrathin ferroelectric films by analysis of synchrotron X-ray scattering measurements. *Phys. Rev. B* 71:144112

93. Egelhoff WF. 1990. X-ray photoelectron and Auger electron forward scattering: a new tool for surface crystallography. *Crit. Rev. Solid State Mater. Sci.* 16:213–35

94. Despont L, Koitzsch C, Clerc F, Garnier MG, Aebi P, et al. 2006. Direct evidence for ferroelectric polar distortion in ultrathin lead titanate perovskite films. *Phys. Rev. B* 73:094110

95. Sirenko AA, Bernhard C, Golnik A, Clark AM, Hao J, et al. 2000. Soft-mode hardening in $SrTiO_3$ thin films. *Nature* 404:373–76

96. Sepliarsky M, Phillpot SR, Stachiotti MG, Migoni RL. 2002. Ferroelectric phase transitions and dynamical behavior in $KNbO_3/KTaO_3$ superlattices by molecular-dynamics simulation. *J. Appl. Phys.* 91:3165–71
97. Barad Y, Lettieri J, Theis CD, Schlom DG, Gopalan V, et al. 2001. Probing domain microstructure in ferroelectric $Bi_4Ti_3O_{12}$ thin films by optical second harmonic generation. *J. Appl. Phys.* 89:1387–92. Erratum. 2001. *J. Appl. Phys.* 89:5230
98. Fiebig M, Fröhlich D, Lottermoser T, Maat M. 2002. Probing of ferroelectric surface and bulk domains in $RMnO_3$ (R = Y, Ho) by second harmonic generation. *Phys. Rev. B* 66:144102
99. Biegalski MD, Jia Y, Schlom DG, Trolier-McKinstry S, Streiffer SK, et al. 2006. Relaxor ferroelectricity in strained epitaxial $SrTiO_3$ thin films on $DyScO_3$ substrates. *Appl. Phys. Lett.* 88:192907
100. Scheel HJ, Bednorz JG, Dill P. 1976. Crystal growth of strontium titanate $SrTiO_3$. *Ferroelectrics* 13:507–9
101. Nabokin PI, Souptel D, Balbashov AM. 2003. Floating zone growth of high-quality $SrTiO_3$ single crystals. *J. Cryst. Growth* 250:397–404
102. Biegalski MD, Trolier-McKinstry S, Schlom DG, Fong DD, Eastman JA, et al. 2007. Structure and critical thickness of semiconductor-grade $SrTiO_3$ films grown on (101) $DyScO_3$. *J. Appl. Phys.* In press
103. Setter N, Damjanovic D, Eng L, Fox G, Gevorgian S, et al. 2006. Ferroelectric thin films: review of materials, properties, and applications. *J. Appl. Phys.* 100:051606
104. Nagarajan V, Jenkins IG, Alpay SP, Li H, Aggarwal S, et al. 1999. Thickness dependence of structural and electrical properties in epitaxial lead zirconate titanate films. *J. Appl. Phys.* 86:595–602
105. Morioka H, Asano G, Oikawa T, Funakubo H, Saito K. 2003. Large remanent polarization of 100% polar-axis-oriented epitaxial tetragonal $Pb(Zr_{0.35}Ti_{0.65})O_3$ thin films. *Appl. Phys. Lett.* 82:4761–63
106. Machlin ES, Chaudhari P. 1980. Theory of 'pseudomorphic stabilization' of metastable phases in thin film form. In *Synthesis and Properties of Metastable Phases*, ed. ES Machlin, TJ Rowland, pp. 11–29. Warrendale, PA: Metall. Soc. AIME
107. Flynn CP. 1986. Strain-assisted epitaxial growth of new ordered compounds. *Phys. Rev. Lett.* 57:599–602
108. Gorbenko OY, Samoilenkov SV, Graboy IE, Kaul AR. 2002. Epitaxial stabilization of oxides in thin films. *Chem. Mater.* 14:4026–43
109. Stringfellow GB, ed. 1992. *Phase Equilibria Diagrams, Vol. 9*. Westerville, OH: Am. Ceram. Soc. 381 pp.
110. Ikeda T. 1959. A few quarternary systems of perovskite type $A^{2+}B^{4+}O^3$ solid solutions. *J. Phys. Soc. Jpn.* 14:1286–94
111. Levin EM, Robbins CR, McMurdie HF, ed. 1964. *Phase Diagrams for Ceramists, Vol. 1*. Columbus, OH: Am. Ceram. Soc. 601 pp.
112. Gutakovskii AK, Fedina LI, Aseev AL. 1995. High resolution electron microscopy of semiconductor interfaces. *Phys. Status Solid. A* 150:127–40

113. Thoma S, Cerva H. 1994. Comparison of the information content in ⟨110⟩- and ⟨100⟩-projected high-resolution transmission electron microscope images for the quantitative analysis of AlAs/GaAs interfaces. *Ultramicroscopy* 53:37–51
114. Li S, Eastman JA, Vetrone JM, Newnham RE, Cross LE. 1997. Dielectric response in ferroelectric superlattices. *Philos. Mag. B* 76:47–57
115. Sai N, Meyer B, Vanderbilt D. 2000. Compositional inversion symmetry breaking in ferroelectric perovskites. *Phys. Rev. Lett.* 84:5636–39
116. Neaton JB, Rabe KM. 2003. Theory of polarization enhancement in epitaxial $BaTiO_3/SrTiO_3$ superlattices. *Appl. Phys. Lett.* 82:1586–88
117. Nakhmanson SM, Rabe KM, Vanderbilt D. 2006. Predicting polarization enhancement in multicomponent ferroelectric superlattices. *Phys. Rev. B* 73:060101
118. Shimuta T, Nakagawara O, Makino T, Arai S, Tabata H, Kawai T. 2002. Enhancement of remanent polarization in epitaxial $BaTiO_3/SrTiO_3$ superlattices with "asymmetric" structure. *J. Appl. Phys.* 91:2290–94
119. Corbett MH, Bowman RM, Gregg JM, Foord DT. 2001. Enhancement of dielectric constant and associated coupling of polarization behavior in thin film relaxor superlattices. *Appl. Phys. Lett.* 79:815–17
120. Kim L, Jung D, Kim J, Kim JS, Lee J. 2003. Strain manipulation in $BaTiO_3/SrTiO_3$ artificial lattice toward high dielectric constant and its nonlinearity. *Appl. Phys. Lett.* 82:2118–20
121. Tian W, Jiang JC, Pan XQ, Haeni JH, Li YL, et al. 2006. Structural evidence for enhanced polarization in a commensurate short-period $BaTiO_3/SrTiO_3$ superlattice. *Appl. Phys. Lett.* 89:092905
122. O'Neill D, Bowman RM, Gregg JM. 2000. Dielectric enhancement and Maxwell-Wagner effects in ferroelectric superlattice structures. *Appl. Phys. Lett.* 77:1520–22
123. Catalan G, O'Neill D, Bowman RM, Gregg JM. 2000. Relaxor features in ferroelectric superlattices: a Maxwell-Wagner approach. *Appl. Phys. Lett.* 77:3078–80
124. Newnham RE, Skinner DP, Cross LE. 1978. Connectivity and piezoelectric-pyroelectric composites. *Mater. Res. Bull.* 13:525–36
125. Zheng H, Wang J, Lofland SE, Ma Z, Mohaddes-Ardabili L, et al. 2004. Multiferroic $BaTiO_3$-$CoFe_2O_4$ nanostructures. *Science* 303:661–63
126. Zheng H, Zhan Q, Zavaliche F, Sherburne M, Straub F, et al. 2006. Controlling self-assembled perovskite-spinel nanostructures. *Nano Lett.* 6:1401–7
127. Ríos S, Ruediger A, Jiang AQ, Scott JF, Lu H, Chen Z. 2003. Orthorhombic strontium titanate in $BaTiO_3$-$SrTiO_3$ superlattices. *J. Phys. Condens. Matter* 15:L305–9
128. Johnston K, Huang XY, Neaton JB, Rabe KM. 2005. First-principles study of symmetry lowering and polarization in $BaTiO_3/SrTiO_3$ superlattices with in-plane expansion. *Phys. Rev. B* 71:100103
129. Tinte S, Rabe KM, Vanderbilt D. 2003. Anomalous enhancement of tetragonality in $PbTiO_3$ induced by negative pressure. *Phys. Rev. B.* 68:144105
130. Stephanovich VA, Luk'yanchuk IA, Karkut MG. 2005. Domain-enhanced interlayer coupling in ferroelectric/paraelectric superlattices. *Phys. Rev. Lett.* 94:047601

131. Neaton JB, Hsueh CL, Rabe KM. 2002. Enhanced polarization in strained $BaTiO_3$ from first principles. In *Perovskite Materials*, ed. K Poeppelmeier, A Navrotsky, R Wentzcovitch, 718:311–16. Warrendale, PA: Mater. Res. Soc.
132. Bungaro C, Rabe KM. 2004. Epitaxially strained [001]-$(PbTiO_3)_1(PbZrO_3)_1$ superlattice and $PbTiO_3$ from first principles. *Phys. Rev. B* 69:184101
133. Antons A, Neaton JB, Rabe KM, Vanderbilt D. 2005. Tunability of the dielectric response of epitaxially strained $SrTiO_3$ from first principles. *Phys. Rev. B* 71:024102
134. Ederer C, Spaldin NA. 2005. Influence of strain and oxygen vacancies on the magnetoelectric properties of multiferroic bismuth ferrite. *Phys. Rev. B* 71:224103
135. Diéguez O, Rabe KM, Vanderbilt D. 2005. First-principles study of epitaxial strain in perovskites. *Phys. Rev. B* 72:144101
136. Ederer C, Spaldin NA. 2005. Effect of epitaxial strain on the spontaneous polarization of thin film ferroelectrics. *Phys. Rev. Lett.* 95:257601
137. Souza I, Iniguez J, Vanderbilt D. 2002. First-principles approach to insulators in finite electric fields. *Phys. Rev. Lett.* 89:117602
138. Diéguez O, Vanderbilt D. 2006. First-principles calculations for insulators at constant polarization. *Phys. Rev. Lett.* 96:056401
139. Front End Processes. 2005. Ferroelectric random access memory (FeRAM). In *The International Technology Roadmap for Semiconductors: 2005*, pp. 54–58. San Jose, CA: Semiconductor Indust. Assoc. Available at **http://www.itrs.net/Links/2005ITRS/Home2005.htm**
140. Matsubara S, Shohata N, Mikami M. 1985. Epitaxial growth of $PbTiO_3$ on $MgAl_2O_4$/Si substrates. *Jpn. J. Appl. Phys.* 24(Suppl. 24–3):10–12
141. Li H, Hu X, Wei Y, Yu Z, Zhang X, et al. 2003. Two-dimensional growth of high-quality strontium titanate thin films on Si. *J. Appl. Phys.* 93:4521–25
142. Walker FJ, McKee RA. 2005. High-k crystalline gate dielectrics: a research perspective. In *High Dielectric Constant Materials: VLSI MOSFET Applications*, ed. HR Huff, DC Gilmer, pp. 607–37. Berlin: Springer
143. Nashimoto K, Fork DK, Ponce FA, Tramontana JC. 1993. Epitaxial $BaTiO_3$/MgO structure grown on GaAs(100) by pulsed laser deposition. *Jpn. J. Appl. Phys.* 32(Pt. 1):4099–102
144. Liang Y, Kulik J, Eschrich TC, Droopad R, Yu Z, Maniar P. 2004. Heteroepitaxy of perovskite oxides on GaAs(001) by molecular beam epitaxy. *Appl. Phys. Lett.* 85:1217–19
145. Cho CR, Hwang JY, Kim JP, Jeong SY, Yoon SG, Lee WJ. 2004. Growth and characterization of $(Ba_{0.5}Sr_{0.5})TiO_3$ films epitaxially grown on (002) GaN/(0006) Al_2O_3 electrode. *Jpn. J. Appl. Phys.* 43(Pt. 2):L1425–28
146. Tian W, Vaithyanathan V, Schlom DG, Zhan Q, Yang SY, et al. 2007. Epitaxial integration of (0001) $BiFeO_3$ with (0001) GaN. *Appl. Phys. Lett.* 90:179208
147. Van Aken BB, Palstra TTM, Filippetti A, Spaldin NA. 2004. The origin of ferroelectricity in magnetoelectric $YMnO_3$. *Nat. Mater.* 3:164–70
148. Fennie CJ, Rabe KM. 2005. Ferroelectric transition in $YMnO_3$ from first principles. *Phys. Rev. B* 72:100103

149. Baltensperger W. 1970. Influence of magnetic order on conduction electrons and phonons in magnetic semiconductors. *J. Appl. Phys.* 41:1052–54
150. Fennie CJ, Rabe KM. 2007. Magnetic and electric phase control in epitaxial $EuTiO_3$ from first principles. *Phys. Rev. Lett.* 97:267602

RELATED RESOURCES

1. Fong DD, Thompson C. 2006. In situ synchrotron X-ray studies of ferroelectric thin films. *Annu. Rev. Mater. Res.* 36:431–65
2. Lines ME, Glass AM. 2001. *Principles and Applications of Ferroelectrics and Related Materials*. Oxford, UK: Oxford University Press. 696 pp.
3. Newnham RE. 2005. *Properties of Materials: Anisotropy, Symmetry, Structure*. Oxford, UK: Oxford University Press. 392 pp.
4. Rabe K, Ahn CH, Triscone JM, eds. 2006. *Modern Ferroelectrics*. Berlin: Springer. 262 pp.
5. Shaw TM, Trolier-McKinstry S, McIntyre PC. 2000. The properties of ferroelectric films at small dimensions. *Annu. Rev. Mater. Res.* 30:263–98
6. Waser R, ed. 2005. *Nanoelectronics and Information Technology: Advanced Electronic Materials and Novel Devices*. Weinheim, Ger.: Wiley-VCH. 995 pp. 2nd ed.

Annual Review of
Materials Research

Volume 37, 2007

Contents

MATERIALS CHARACTERIZATION

FERROELECTRICS AND RELATED MATERIALS, *David R. Clarke and Venkatraman Gopalan, Guest Editors*

Index

Errata

An online log of corrections to *Annual Review of Materials Research* chapters (if any, 1997 to the present) may be found at http://matsci.annualreviews.org/errata.shtml